

# Regime-Adaptive Bayesian Optimization via Dirichlet Process Mixtures of Gaussian Processes

**Yan Zhang**

*Department of Computer Science, Florida State University*

YZ18B@FSU.EDU

**Xuefeng Liu**

*Department of Computer Science, University of Chicago*

XUEFENG@UCHICAGO.EDU

**Sipeng Chen**

*Department of Computer Science, Florida State University*

SC25BG@FSU.EDU

**Sascha Ranftl**

*School of Mechanical Engineering, Purdue University*

SASCHA\_RANFTL@BROWN.EDU

**Chong Liu**

*College of Nanotechnology, Science, and Engineering, State University of New York at Albany*

CLIU24@ALBANY.EDU

**Shibo Li\***

*Department of Computer Science, Florida State University*

SHIBOLI@CS.FSU.EDU

## Abstract

Standard Bayesian Optimization (BO) assumes uniform smoothness across the search space—an assumption violated in multi-regime problems such as molecular conformation search through distinct energy basins or drug discovery across heterogeneous molecular scaffolds. A single GP either oversmooths sharp transitions or hallucinates noise in smooth regions, yielding miscalibrated uncertainty. We propose RAMBO, a Dirichlet Process Mixture of Gaussian Processes that automatically discovers latent regimes during optimization, each modeled by an independent GP with locally-optimized hyperparameters. We derive collapsed Gibbs sampling that analytically marginalizes latent functions for efficient inference, and introduce adaptive concentration parameter scheduling for coarse-to-fine regime discovery. Our acquisition functions decompose uncertainty into intra-regime and inter-regime components. Experiments on synthetic benchmarks and real-world applications—including molecular conformer optimization, virtual screening for drug discovery, and fusion reactor design—demonstrate consistent improvements over state-of-the-art baselines on multi-regime objectives. Our implementation is publicly available at <https://github.com/AnthonyZhangYan/RAMBO>.

## 1. Introduction

Bayesian Optimization (BO) has become the standard approach for optimizing expensive black-box functions, with applications spanning hyperparameter tuning (Snoek et al., 2012; Feurer and Hutter, 2019), neural architecture search (Zoph and Le, 2017; Elsken et al., 2019; Kandasamy et al., 2018), materials discovery (Lookman et al., 2019; Xue et al., 2016; Kusne et al., 2020), and drug design (Gómez-Bombarelli et al., 2018; Sanchez-Lengeling

---

\*. Corresponding author.

and Aspuru-Guzik, 2018). By fitting a Gaussian Process (GP) surrogate to observed data  $\mathcal{D}$  (Rasmussen, 2003) and using acquisition functions to guide sampling (Jones et al., 1998; Mockus, 1998), BO efficiently navigates high-dimensional spaces with minimal function evaluations.

However, standard BO with stationary kernels assumes uniform smoothness and noise characteristics across the search space. While non-stationary kernel constructions exist—such as input-dependent length scales (Paciorek and Schervish, 2003; Higdon et al., 1999; Plagemann et al., 2008) or deep GP compositions (Damianou and Lawrence, 2013; Wilson et al., 2016a)—they model smoothly-varying hyperparameters and require specifying the functional form of this variation *a priori*. In contrast, many scientific design problems exhibit discrete regime structure with abrupt transitions rather than gradual parameter drift. In molecular conformation search (Hawkins et al., 2010; Riniker and Landrum, 2015), rotatable bonds create distinct energy basins separated by torsional barriers—each basin locally smooth, but the global landscape comprising hundreds of such basins with incommensurable curvature. Drug discovery landscapes (Gómez-Bombarelli et al., 2018; Griffiths and Hernández-Lobato, 2020; Korovina et al., 2020) are fragmented across molecular scaffolds, where different chemical families exhibit fundamentally different structure-activity relationships. Fusion reactor design (Gates et al., 2018; Cadena et al., 2025) traverses qualitatively different stability regimes as plasma geometry varies. In each domain, the objective function is not a smooth surface with slowly-varying properties but a patchwork of locally coherent regions separated by sharp boundaries. This discrete heterogeneity is poorly captured by continuous non-stationary kernels, which must interpolate smoothly between regimes and cannot represent the abrupt transitions that characterize real scientific landscapes. A mixture model, by contrast, naturally represents this structure: each component captures a distinct regime with its own hyperparameters, while the probabilistic assignment mechanism identifies regime boundaries directly from data without requiring their functional form to be specified in advance.

Building on this insight, we propose *Regime-Adaptive Mixture Bayesian Optimization* (RAMBO), which replaces the monolithic GP surrogate with a Dirichlet Process Mixture Model of Gaussian Processes (DPMM-GP). This nonparametric Bayesian framework adaptively partitions the search space into an unknown number of regimes inferred directly from data, with each regime modeled by an independent GP with locally-optimized hyperparameters. The Dirichlet Process prior provides automatic model selection: given  $n$  observations, the expected number of discovered regimes  $K$  grows as  $\mathbb{E}[K \mid n] \approx \alpha \log(n/\alpha + 1)$  (Antoniak, 1974), adapting complexity to data without manual specification. We further introduce **adaptive concentration parameter scheduling** to control regime discovery dynamics throughout optimization. The concentration parameter  $\alpha$  governs the propensity to create new regimes, and its optimal value varies with the amount of available data. Early stages benefit from small  $\alpha$  to avoid premature fragmentation when observations are sparse; later stages permit larger  $\alpha$  to discover fine-grained structure as evidence accumulates. This scheduling mirrors the exploration-exploitation tradeoff inherent to BO, but operates at the model complexity level rather than the sampling location level. Our contributions are as follows:

- We develop a complete DPMM-GP surrogate for BO with collapsed Gibbs sampling that analytically marginalizes latent functions, improving mixing efficiency over HMC-based inference (Rasmussen and Ghahramani, 2001).
- We introduce adaptive  $\alpha$ -scheduling to dynamically adjust model complexity—starting with small  $\alpha$  to avoid premature fragmentation, then increasing to enable fine-grained regime discovery as data accumulates.
- We derive closed-form Expected Improvement for the DPMM-GP posterior, naturally decomposing uncertainty into intra-regime variance and inter-regime disagreement.
- We conduct extensive experiments on synthetic benchmarks and scientific applications—molecular conformer optimization, virtual screening for drug discovery, and fusion reactor design—demonstrating consistent improvements over state-of-the-art baselines on multi-regime objectives.

## 2. Background

**Gaussian Processes.** A Gaussian Process (GP) defines a distribution over functions  $f(\mathbf{x})$  (Rasmussen, 2003; Williams and Rasmussen, 1995; MacKay et al., 1998), fully specified by a mean function  $m(\mathbf{x})$  and covariance (kernel) function  $k(\mathbf{x}, \mathbf{x}')$ , written  $f(\mathbf{x}) \sim \mathcal{GP}(m(\mathbf{x}), k(\mathbf{x}, \mathbf{x}'))$ . In BO, we typically assume a zero-mean prior and use stationary kernels (Genton, 2001; Schölkopf and Smola, 2002) such as the Squared Exponential (SE):  $k(\mathbf{x}, \mathbf{x}') = \sigma_f^2 \exp\left(-\frac{\|\mathbf{x} - \mathbf{x}'\|^2}{2\ell^2}\right)$ , where  $\sigma_f^2$  is the signal variance and  $\ell$  is the length scale controlling smoothness or Matérn (Matérn, 1960). Given observations  $\mathcal{D}_n = \{(\mathbf{x}_i, y_i)\}_{i=1}^n$  with  $y_i = f(\mathbf{x}_i) + \epsilon_i$  and  $\epsilon_i \sim \mathcal{N}(0, \sigma_n^2)$ , the posterior at a test point  $\mathbf{x}_*$  is Gaussian:  $p(f(\mathbf{x}_*) \mid \mathcal{D}_n) = \mathcal{N}(\mu_n(\mathbf{x}_*), \sigma_n^2(\mathbf{x}_*))$ , with  $\mu_n(\mathbf{x}_*) = \mathbf{k}_*^\top (\mathbf{K} + \sigma_n^2 \mathbf{I})^{-1} \mathbf{y}$ ;  $\sigma_n^2(\mathbf{x}_*) = k(\mathbf{x}_*, \mathbf{x}_*) - \mathbf{k}_*^\top (\mathbf{K} + \sigma_n^2 \mathbf{I})^{-1} \mathbf{k}_*$ , where  $\mathbf{K}$  is the kernel matrix with  $K_{ij} = k(\mathbf{x}_i, \mathbf{x}_j)$  and  $\mathbf{k}_* = [k(\mathbf{x}_1, \mathbf{x}_*), \dots, k(\mathbf{x}_n, \mathbf{x}_*)]^\top$ . Computing the matrix inverse requires  $\mathcal{O}(n^3)$  operations, but this is tractable in BO where  $n$  is typically small. The critical limitation is that the hyperparameters  $\theta = \{\ell, \sigma_f^2, \sigma_n^2\}$  are global: if the function varies rapidly in one region and slowly in another, a single GP estimates a compromise length scale that performs poorly in both.

**Bayesian Optimization.** BO (Mockus, 1998; Brochu et al., 2010; Shahriari et al., 2016; Frazier, 2018) seeks the global optimum of an expensive black-box function:  $\mathbf{x}^* = \operatorname{argmax}_{\mathbf{x} \in \mathcal{X}} f(\mathbf{x})$ , where  $f : \mathcal{X} \rightarrow \mathbb{R}$  is costly to evaluate,  $\mathcal{X} \subseteq \mathbb{R}^d$  is a compact domain, and observations are noisy:  $y = f(\mathbf{x}) + \epsilon$ , where  $\epsilon \sim \mathcal{N}(0, \sigma_n^2)$ . The framework proceeds iteratively: (1) fit a probabilistic surrogate (typically a GP) to observed data  $\mathcal{D}_t$ ; (2) select the next query point by maximizing an acquisition function  $\alpha(\mathbf{x})$  that balances exploration and exploitation; (3) evaluate  $f$  at the selected point and update  $\mathcal{D}_{t+1}$ . Common acquisition functions include Expected Improvement (EI) (Jones et al., 1998; Mockus, 1998), which quantifies expected gain over the current best  $f^+ = \max_i y_i$ :  $\text{EI}(\mathbf{x}) = \mathbb{E}[\max(0, f(\mathbf{x}) - f^+)] = \sigma(\mathbf{x}) [\gamma \Phi(\gamma) + \phi(\gamma)]$ , where  $\gamma = (\mu(\mathbf{x}) - f^+)/\sigma(\mathbf{x})$  and  $\Phi, \phi$  denote the standard normal CDF and PDF. Upper Confidence Bound (UCB) (Srinivas et al., 2010; Auer et al., 2002) selects optimistically:  $\text{UCB}(\mathbf{x}) = \mu(\mathbf{x}) + \beta_t^{1/2} \sigma(\mathbf{x})$ , where  $\beta_t$  is a theoretically-guided exploration parameter. Thompson Sampling (Thompson, 1933; Russo et al., 2018) draws a function  $\tilde{f} \sim p(f \mid \mathcal{D}_t)$  from the posterior and optimizes it directly.

**Dirichlet Process and Mixture Models** The Dirichlet Process (DP) (Ferguson, 1973; Antoniak, 1974) serves as the cornerstone of Bayesian nonparametric modeling, providing a distribution over probability measures with support on an infinite sample space. It is rigorously defined via its finite-dimensional marginals.

**Definition 1 (Dirichlet Process)** Let  $(\Omega, \mathcal{F})$  be a measurable space and  $G_0$  a probability measure on  $\Omega$ . A random probability measure  $G$  is distributed according to a Dirichlet process with concentration parameter  $\alpha > 0$  and base measure  $G_0$ , denoted  $G \sim \text{DP}(\alpha, G_0)$ , if for every finite measurable partition  $(A_1, \dots, A_K)$  of  $\Omega$ , the vector of random probabilities follows a Dirichlet distribution:  $(G(A_1), \dots, G(A_K)) \sim \text{Dir}(\alpha G_0(A_1), \dots, \alpha G_0(A_K))$ . The parameter  $\alpha$  governs the variance of the process; as  $\alpha \rightarrow \infty$ ,  $G$  converges weakly to  $G_0$ .

While Definition 1 establishes the existence of the process, it does not offer a direct method for sampling. The *stick-breaking construction* provides an explicit generative representation, proving that realizations of a DP are almost surely discrete.

**Theorem 2 (Sethuraman's Stick-Breaking Construction (Sethuraman, 1994))** A random measure  $G \sim \text{DP}(\alpha, G_0)$  admits the almost sure representation:

$$G = \sum_{k=1}^{\infty} \pi_k \delta_{\theta_k},$$

where the atoms  $\theta_k \stackrel{i.i.d.}{\sim} G_0$  and the weights  $\{\pi_k\}$  are generated via:  $\beta_k \sim \text{Beta}(1, \alpha)$ ;  $\pi_k = \beta_k \prod_{j=1}^{k-1} (1 - \beta_j)$ .

This construction elucidates the clustering property of the DP: since  $G$  is discrete, multiple observations  $\theta_i \sim G$  will share identical values with non-zero probability. The number of unique values (clusters), denoted  $K_n$ , grows logarithmically with the dataset size  $n$ , allowing model complexity to adapt automatically to the data.

**Theorem 3 (Expected Number of Clusters)** For a sample of size  $n$ , the expected number of distinct clusters satisfies:

$$\mathbb{E}[K_n \mid \alpha] = \sum_{i=1}^n \frac{\alpha}{i-1+\alpha} \approx \alpha \log \left( 1 + \frac{n}{\alpha} \right).$$

While the stick-breaking view describes the conditional distribution of observations given  $G$ , the *Chinese Restaurant Process* (CRP) describes the marginal distribution of cluster assignments obtained by integrating out  $G$ .

**Definition 4 (Chinese Restaurant Process)** Given assignments  $z_{1:n-1}$ , for each existing cluster  $k \in \{1, \dots, K_{n-1}\}$ ,

$$p(z_n = k \mid z_{1:n-1}, \alpha) = \frac{n_k}{n-1+\alpha},$$

and the probability of creating a new cluster is

$$p(z_n = K_{n-1} + 1 \mid z_{1:n-1}, \alpha) = \frac{\alpha}{n-1+\alpha},$$

where  $n_k = \#\{i < n : z_i = k\}$ .

The CRP exhibits a rich-get-richer property (Pitman and Yor, 1997): popular clusters attract more members, inducing power-law cluster sizes. Combining these elements, a Dirichlet Process Mixture Model (DPMM) (Escobar and West, 1995; Neal, 2000; McLachlan and Peel, 2000) places a DP prior over mixture components:  $G \sim \text{DP}(\alpha, G_0)$ ,  $\theta_i \sim G$ , and  $x_i \sim F(\theta_i)$  for some parametric family  $F$ . The resulting model has infinitely many potential components but instantiates only finitely many for any finite dataset.

### 3. Probabilistic Surrogate for RAMBO

#### 3.1 Generative Process of DPMM

The Dirichlet Process Mixture of Gaussian Processes (DPMM-GP) models the objective as a countable mixture of independent GPs, partitioning the search space into latent “regimes” that adapt to non-stationarity and heteroscedasticity. Let  $\alpha > 0$  denote the concentration parameter and  $G_0(\theta)$  the base measure over kernel hyperparameters. The generative process first constructs mixture weights via stick-breaking:  $\beta_k \sim \text{Beta}(1, \alpha)$  with  $\pi_k = \beta_k \prod_{j < k} (1 - \beta_j)$ . Each regime  $k$  is then assigned hyperparameters  $\theta_k = \{\sigma_{f,k}^2, \ell_k, \sigma_{n,k}^2\} \sim G_0$ . For each observation  $i$ , we draw a latent assignment  $z_i \sim \text{Categorical}(\{\pi_k\}_{k=1}^\infty)$ , then generate the observation from the corresponding GP:  $f_k \sim \mathcal{GP}(0, k_{\theta_k})$  and  $y_i | z_i = k \sim \mathcal{N}(f_k(\mathbf{x}_i), \sigma_{n,k}^2)$ .

This hierarchical structure allows distinct components to capture qualitatively different local characteristics. The signal variance  $\sigma_{f,k}^2$  governs the output amplitude, the length scale  $\ell_k$  dictates the function’s local smoothness, and  $\sigma_{n,k}^2$  captures the local observation noise variance within regime  $k$ . For computational tractability, the base distribution  $G_0$  is factorized as a product of independent Inverse-Gamma priors (Gelman et al., 2013), which provide conjugacy to the Gaussian likelihoods:  $\sigma_{f,k}^2 \sim \text{InvGamma}(a_f, b_f)$ ;  $\ell_k \sim \text{InvGamma}(a_\ell, b_\ell)$ ;  $\sigma_{n,k}^2 \sim \text{InvGamma}(a_n, b_n)$ . The hyperparameters for these priors are calibrated empirically based on the data range. We set the shape parameters  $a_f = a_\ell = a_n = 2$  to ensure finite means, while the scale parameters  $b_f, b_\ell, b_n$  are adjusted according to the empirical variance and input domain bounds.

**Joint Distribution and Marginal Likelihood** We now formalize the generative structure and derive the marginal likelihood required for inference. The joint probability density of the DPMM-GP decomposes into the nonparametric prior over the mixture components and the conditional likelihood of the observations.

**Theorem 5 (DPMM-GP Joint Distribution)** *Given the hyperparameters  $\{\alpha, G_0\}$  and input data  $\mathbf{X}$ , the joint distribution over the latent variables and observations factorizes as:*

$$p(\mathbf{y}, \mathbf{z}, \Theta, \mathbf{f} | \mathbf{X}) = \left[ \prod_{k=1}^{\infty} p(\beta_k | \alpha) p(\theta_k | G_0) p(f_k | \theta_k) \right] \times \prod_{i=1}^n \underbrace{p(z_i | \boldsymbol{\beta})}_{\pi_{z_i}} \underbrace{p(y_i | f_{z_i}(\mathbf{x}_i), \theta_{z_i})}_{\mathcal{N}(y_i | \dots)} \quad (1)$$

where  $\Theta = \{\theta_k, \beta_k\}_{k=1}^\infty$  represents the global parameters.

A structural advantage of this model is the analytic tractability of the Gaussian Process. Since the GP prior is conjugate to the Gaussian likelihood, we can analytically integrate out the latent function values  $\mathbf{f}$  to obtain a closed-form marginal likelihood for each cluster.

**Proposition 6 (Cluster Marginal Likelihood)** *Let  $\mathbf{y}_k$  and  $\mathbf{X}_k$  denote the subset of observations assigned to regime  $k$ . The marginal likelihood for this cluster, conditioned on hyperparameters  $\theta_k$ , is:*

$$p(\mathbf{y}_k \mid \mathbf{X}_k, \theta_k) = \mathcal{N}(\mathbf{y}_k \mid \mathbf{0}, \mathbf{K}_k + \sigma_{n,k}^2 \mathbf{I}), \quad (2)$$

where  $[\mathbf{K}_k]_{ij} = k_{\theta_k}(\mathbf{x}_i, \mathbf{x}_j)$  is the kernel matrix evaluated on  $\mathbf{X}_k$ .

**Proof** The result follows from the standard convolution of Gaussians. The marginalization of the latent function  $f_k$  is defined as:

$$\int \mathcal{N}(\mathbf{y}_k \mid \mathbf{f}_k, \sigma_{n,k}^2 \mathbf{I}) \mathcal{N}(\mathbf{f}_k \mid \mathbf{0}, \mathbf{K}_k) d\mathbf{f}_k. \quad (3)$$

Using standard Gaussian identities, the sum of independent Gaussian variables (signal  $f_k$  plus noise  $\varepsilon$ ) yields a Gaussian with covariance  $\mathbf{K}_k + \sigma_{n,k}^2 \mathbf{I}$ .  $\blacksquare$

This closed-form marginalization reduces the inference problem to sampling only the discrete assignments  $\mathbf{z}$  and hyperparameters  $\Theta$ , significantly improving MCMC mixing rates.

### 3.2 Posterior Inference via Collapsed Gibbs Sampling

Direct optimization of the DPMM-GP objective is intractable due to the discrete nature of the regime assignments and the trans-dimensional parameter space (the number of regimes  $K$  is not fixed). Furthermore, standard Gibbs sampling schemes (Neal, 2000) that instantiate the latent function values  $\mathbf{f}$  suffer from severe autocorrelation, as the strong coupling between  $\mathbf{f}$  and  $\mathbf{z}$  inhibits mixing (Liu, 1994; Neal, 2000; Ishwaran and James, 2001). By analytically marginalizing out  $\mathbf{f}$  (Theorem 5), we reduce the state space to only the assignments  $\mathbf{z}$  and hyperparameters  $\Theta$ . This ‘‘collapsed’’ scheme significantly improves mixing efficiency while retaining the ability to explore the multimodal posterior distribution of the partition structure.

**Sampling Regime Assignments** For each observation  $i$ , we sample a new assignment  $z_i$  conditioned on all other variables. The conditional probability of assigning observation  $i$  to regime  $k$  is proportional to the product of the CRP prior and the conditional likelihood:

$$p(z_i = k \mid \mathbf{z}_{-i}, \mathcal{D}) \propto \underbrace{p(z_i = k \mid \mathbf{z}_{-i}, \alpha)}_{\text{CRP Prior}} \times \underbrace{p(y_i \mid \mathbf{x}_i, \mathcal{D}_{k,-i}, \theta_k)}_{\text{Likelihood}}.$$

Depending on the regime index  $k$ , this probability takes two forms:

1. **Existing Regime ( $k \leq K$ ):** The prior probability is proportional to  $n_{k,-i}$ , the count of current members excluding  $i$ . The likelihood term is the GP posterior predictive density conditioned on the existing data in regime  $k$ :

$$p(y_i \mid \dots) = \mathcal{N}(y_i \mid \mu_{i|k}, \sigma_{i|k}^2), \quad (4)$$

where  $\mu_{i|k}$  and  $\sigma_{i|k}^2$  are the standard GP predictive mean and variance given  $\mathcal{D}_{k,-i}$ .

2. **New Regime ( $k = K + 1$ ):** The prior probability is proportional to  $\alpha$ . The likelihood is the marginal probability under  $G_0$ . We approximate this via Monte Carlo integration:

$$p(y_i | \mathbf{x}_i, G_0) \approx \frac{1}{M} \sum_{m=1}^M \mathcal{N}(y_i | 0, \sigma_{tot}^{2(m)}), \quad (5)$$

where  $\sigma_{tot}^{2(m)} = k_{\theta^{(m)}}(\mathbf{x}_i, \mathbf{x}_i) + \sigma_{n^{(m)}}^2$  represents the total variance for sample  $\theta^{(m)} \sim G_0$ .

**Updating Hyperparameters** Given the assignments  $\mathbf{z}$ , the hyperparameters for each active regime are independent. We update  $\theta_k$  by targeting the posterior  $p(\theta_k | \mathcal{D}_k) \propto p(\mathbf{y}_k | \theta_k)p(\theta_k | G_0)$ . In our experiments, we adopt an empirical Bayes approach, maximizing the log-marginal likelihood w.r.t.  $\theta_k$  using Adam (Kingma and Ba, 2015) for computational efficiency. Alternatively, a fully Bayesian treatment can be achieved via Metropolis-Hastings (Hastings, 1970) steps with log-normal proposals, accepting updates based on the marginal likelihood ratio. We defer the complete inference procedure to Algorithm 1 in the Appendix B.1.

### 3.3 Posterior Predictive Distribution

The posterior predictive distribution for a new test point  $\mathbf{x}_*$  is obtained by marginalizing over the latent regime assignments and regime-specific parameters. This results in a finite mixture of Gaussian Process posteriors.

**Theorem 7 (Posterior Predictive Density)** *The predictive density for a test input  $\mathbf{x}_*$ , conditioned on the training data  $\mathcal{D}$ , is given by:*

$$p(y_* | \mathbf{x}_*, \mathcal{D}) = \sum_{k=1}^{K+1} w_k(\mathbf{x}_*) \cdot \mathcal{N}(y_* | \mu_{*,k}, \sigma_{*,k}^2), \quad (6)$$

where  $(\mu_{*,k}, \sigma_{*,k}^2)$  denote the GP posterior predictive mean and variance for regime  $k$ .

The gating weights  $w_k(\mathbf{x}_*) \approx p(z_* = k | \mathbf{x}_*, \mathcal{D})$  represent the assignment probability for the test point. In our framework, this weight modulates the non-parametric CRP prior with a local confidence score:

$$w_k(\mathbf{x}_*) \propto \frac{n_k}{n + \alpha} \cdot \exp\left(-\frac{1}{2} \log \sigma_{*,k}^2(\mathbf{x}_*)\right). \quad (7)$$

The first term,  $\frac{n_k}{n + \alpha}$ , enforces the ‘rich-get-richer’ property of the Dirichlet Process, favoring large, established clusters. The second term functions as a spatial likelihood, penalizing regimes that exhibit high predictive uncertainty at  $\mathbf{x}_*$ . Consequently, the model assigns  $\mathbf{x}_*$  to regimes that are both populous and confident (low variance) in the local vicinity of the test point.

**Theorem 8 (Moment Matching)** *The mean  $\mu_{mix}$  and variance  $\sigma_{mix}^2$  of the predictive mixture are:*

$$\mu_{mix}(\mathbf{x}_*) = \sum_{k=1}^{K+1} w_k(\mathbf{x}_*) \mu_{*,k}, \quad (8)$$

$$\sigma_{mix}^2(\mathbf{x}_*) = \sum_{k=1}^{K+1} w_k(\mathbf{x}_*) [\sigma_{*,k}^2 + \mu_{*,k}^2] - \mu_{mix}^2. \quad (9)$$

**Proof** We apply the laws of total expectation and variance. Let  $Z$  be the indicator variable for the regime assignment.

1.  $\mathbb{E}[y_*] = \mathbb{E}_Z[\mathbb{E}[y_* | Z]] = \sum_k w_k \mu_{*,k}.$
2.  $\text{Var}[y_*] = \mathbb{E}_Z[\text{Var}[y_* | Z]] + \text{Var}_Z[\mathbb{E}[y_* | Z]].$

Substituting the component moments:

$$\begin{aligned}\sigma_{\text{mix}}^2 &= \sum_k w_k \sigma_{*,k}^2 + \left( \sum_k w_k \mu_{*,k}^2 - \left( \sum_k w_k \mu_{*,k} \right)^2 \right) \\ &= \sum_k w_k (\sigma_{*,k}^2 + \mu_{*,k}^2) - \mu_{\text{mix}}^2.\end{aligned}\tag{10}$$

■

This variance decomposition highlights two distinct sources of uncertainty. The first term,  $\sum w_k \sigma_{*,k}^2$ , represents the **intra-regime uncertainty** (average GP variance). The second term,  $\text{Var}_Z[\mu]$ , captures the **inter-regime disagreement** (variance of the means). This ensures robust uncertainty quantification: even if individual regimes are confident, the model reports high overall uncertainty if the regimes disagree on the prediction.

#### 4. Acquisition Functions

To guide the optimization process, we must map the posterior predictive distribution to a scalar utility value. We prioritize Expected Improvement (EI) due to its analytic tractability and robustness to the non-stationary scaling inherent in our mixture model.

**Mixture Expected Improvement** In the DPMM-GP framework, different latent regimes often exhibit vastly different signal variances ( $\sigma_{f,k}^2$ ). A regime modeling a “flat” region may have small variance, while a “rough” regime has large variance. Metric-based acquisition functions like UCB require a trade-off parameter  $\beta_t$  that is difficult to calibrate across these heterogeneous scales.

In contrast, Expected Improvement naturally adapts to local scaling. It quantifies the expected gain over the current best observation  $f^+ = \max_i y_i$ , weighted by the probability of the latent regime assignment.

**Theorem 9 (DPMM-GP Expected Improvement)** *The Expected Improvement at input  $\mathbf{x}$  is the probability-weighted sum of the EI for each constituent GP component:*

$$\alpha_{EI}(\mathbf{x}) = \sum_{k=1}^K w_k(\mathbf{x}) \cdot \sigma_{*,k}(\mathbf{x}) [\gamma_k \Phi(\gamma_k) + \phi(\gamma_k)],\tag{11}$$

where  $\gamma_k = (\mu_{*,k}(\mathbf{x}) - f^+)/\sigma_{*,k}(\mathbf{x})$  is the normalized improvement  $Z$ -score for regime  $k$ , and  $\Phi, \phi$  are the standard normal CDF and PDF, respectively.

**Proof** The result follows from the Law of Total Expectation. Let  $I(\mathbf{x}) = \max(0, f(\mathbf{x}) - f^+)$  be the improvement utility. Conditioning on the latent assignment variable  $z_*$ :

$$\mathbb{E}[I(\mathbf{x})] = \mathbb{E}_{z_*} [\mathbb{E}[I(\mathbf{x}) \mid z_*]] \quad (12)$$

$$= \sum_{k=1}^K p(z_* = k \mid \mathbf{x}) \cdot \mathbb{E}_{\text{GP}_k}[I(\mathbf{x})] \quad (13)$$

$$= \sum_{k=1}^K w_k(\mathbf{x}) \cdot \text{EI}_k(\mathbf{x}). \quad (14)$$

Since each conditional component  $p(f \mid z_* = k)$  is Gaussian, the inner term  $\text{EI}_k(\mathbf{x})$  reduces to the standard closed-form GP-EI formula.  $\blacksquare$

This formulation encourages a balanced search strategy: the acquisition value is high if a point belongs to a regime that predicts high improvement, or if there is significant ambiguity about the regime assignment itself (via weights  $w_k$ ), necessitating exploration to resolve the structural uncertainty.

**Adaptive Concentration Parameter Scheduling** The concentration parameter  $\alpha$  governs regime creation: larger  $\alpha$  encourages more clusters, with  $\mathbb{E}[K_n \mid \alpha] \approx \alpha \log(n/\alpha + 1)$  (Antoniak, 1974). Prior work either fixes  $\alpha$  or learns it via MCMC (Rasmussen and Ghahramani, 2001), but for sequential optimization, the appropriate  $\alpha$  varies with data availability—early stages benefit from small  $\alpha$  to avoid premature fragmentation when observations are sparse, while later stages permit larger  $\alpha$  to discover fine-grained structure as evidence accumulates. We formalize this intuition by deriving a schedule that matches the prior’s expected complexity to a polynomial regime discovery rate  $\mathcal{O}(n^\beta)$ . Setting  $\beta = 1/2$ , motivated by square-root growth laws observed in clustering and information retrieval (Heaps, 1978), yields the **Log-Sqrt Schedule**:

$$\alpha_t = \alpha_0 \cdot \frac{\sqrt{t}}{\log(t + e)}, \quad (15)$$

where  $\alpha_0 = 0.2$  is the base concentration. This schedule enforces early parsimony, enables progressive refinement, and balances bias-variance throughout optimization. The full derivation is provided in Appendix D.

**Acquisition Optimization** The acquisition landscape of the DPMM-GP is inherently multimodal, inheriting local optima from the superposition of multiple regime-specific GP posteriors. Consequently, standard convex optimization is insufficient. We maximize  $\alpha(\mathbf{x})$  using a multi-start L-BFGS-B strategy (Wilson et al., 2018) with automatic differentiation. To ensure robust convergence, the optimizer is initialized with a hybrid set of candidates  $\mathcal{S}_{\text{init}}$  comprising: (1) a dense set of uniform random samples from  $\mathcal{X}$  to encourage global exploration, (2) the centroids of currently active regimes to exploit high-probability regions, and (3) local Gaussian perturbations around the current best observation  $\mathbf{x}^*$ . The complete optimization loop is detailed in Algorithm 2 (Appendix B.2). While we prioritize EI for its parameter-free formulation and natural robustness to the heterogeneous scales, the

closed-form mixture moments derived in Theorem 8 enable seamless extension to other standard acquisition functions—including UCB, Thompson Sampling, Max-value Entropy Search (Wang and Jegelka, 2017), Knowledge Gradient (KG) (Frazier et al., 2009), Predictive Entropy Search (PES) and Probability of Improvement (Kushner, 1964)—without additional approximation (see Appendix A for details).

## 5. Related Work

Modern Bayesian optimization (BO) is founded on Expected Improvement (Jones et al., 1998) and the theoretical regret bounds of GP-UCB (Srinivas et al., 2010; Scarlett et al., 2017; Chowdhury and Gopalan, 2017), with practical adoption driven by efficient GP implementations (Snoek et al., 2012). Standard acquisition strategies have expanded to include Thompson Sampling (Thompson, 1933; Russo et al., 2018), Knowledge Gradient (Frazier et al., 2009; Wu and Frazier, 2016), and entropy-based search (Hennig and Schuler, 2012; Wang and Jegelka, 2017; Hernández-Lobato et al., 2014). While robust, these methods typically assume stationary surrogates. To address scalability and high-dimensionality, recent approaches employ local trust regions (TuRBO (Eriksson et al., 2019), SCBO (Eriksson and Poloczek, 2021)), dimensionality reduction via embeddings (REMBO (Wang et al., 2016), ALEBO (Letham et al., 2020), BAxUS (Papenmeier et al., 2022)), or structural priors (SAASBO (Eriksson and Jankowiak, 2021), Add-GP-UCB (Kandasamy et al., 2015)). Although recent studies (Xu et al., 2025; Hvarfner et al., 2024) suggest standard GPs with proper initialization can rival these specialized methods, they do not resolve the limitations of stationarity in heterogeneous landscapes. Multi-fidelity methods (Poloczek et al., 2017; Takeno et al., 2020; Huang et al., 2006; Kandasamy et al., 2016; Li et al., 2020, 2021) exploit cheap approximations to accelerate optimization, though they assume consistent structure across fidelity levels. Parallel advances extend BO to mixed-variable and combinatorial spaces using random forests (Hutter et al., 2011; Bergstra et al., 2011), tree-structured estimators (Bergstra et al., 2011; Falkner et al., 2018), and graph kernels (Oh et al., 2019; Wan et al., 2021; Garrido-Merchán and Hernández-Lobato, 2020; Deshwal and Doppa, 2021; Ru et al., 2020). Specific remedies for non-stationarity include input warping (HEBO (Cowen-Rivers et al., 2022), Warped GPs (Snoek et al., 2014)), Deep GPs (Damianou and Lawrence, 2013; Wilson et al., 2016b), input-dependent kernels (Paciorek and Schervish, 2003), neural surrogates (Snoek et al., 2015; Springenberg et al., 2016; White et al., 2021), and axis-aligned partitioning via Treed GPs (Gramacy and Lee, 2008). However, these approaches generally rely on single global models or hard geometric partitions, failing to quantify the probabilistic uncertainty inherent in natural regime boundaries. *Most related* to our work is the Infinite Mixture of GP Experts (Rasmussen and Ghahramani, 2001), with other formulations explored in (Tresp, 2000; Meeds and Osindero, 2005; Yuan and Neubauer, 2008; Nguyen and Bonilla, 2014). The critical distinction is in the gating mechanism: Rasmussen & Ghahramani employ an *input-dependent* gating network that conditions regime assignment on spatial location, requiring explicit learning of gating boundaries. Our framework instead uses an *input-independent* Chinese Restaurant Process prior, letting the *marginal likelihood* of local GPs naturally induce spatial partitioning—points in coherent regions exhibit higher likelihood under a shared smooth function, eliminating the overhead of learning explicit boundaries. RAMBO adapts this non-parametric philosophy specifically

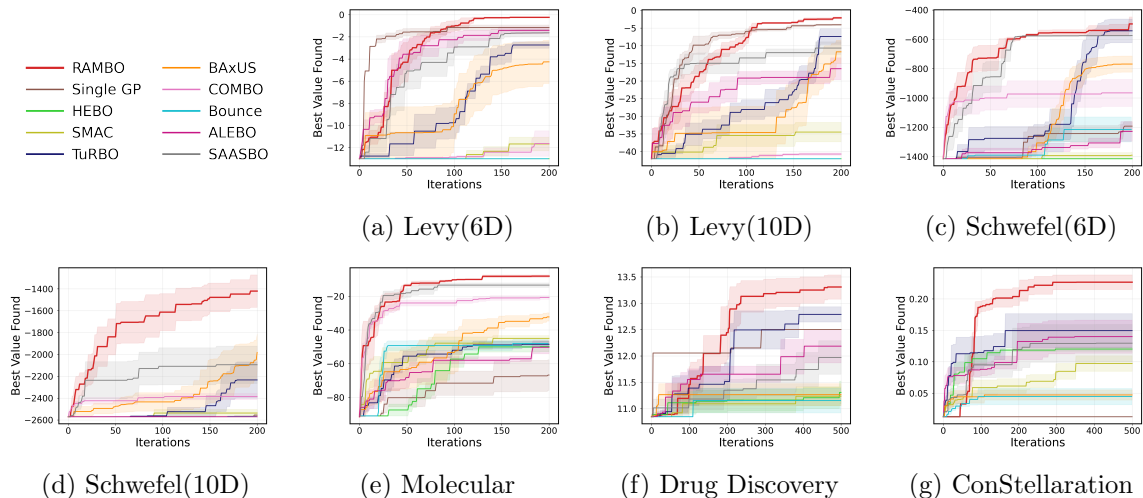


Figure 1: Optimization performance across synthetic and real-world benchmarks. We report the best objective value found (mean  $\pm$  SE over 5 seeds). (a)–(d) Levy and Schwefel functions in 6D and 10D. (e)–(g) Molecular conformer optimization (12D), virtual screening for drug discovery (50D), and stellarator reactor design (81D). RAMBO consistently matches or outperforms all baselines, with the largest gains on *high-dimensional, multi-regime* landscapes.

for Bayesian Optimization through regime-aware acquisition functions—decomposing uncertainty into intra-regime aleatoric variance and inter-regime epistemic disagreement—and adaptive  $\alpha$ -scheduling that enforces parsimony early while enabling fine-grained regime discovery as data accumulates.

## 6. Experiments

We evaluate RAMBO against state-of-the-art Bayesian optimization baselines across tasks spanning synthetic functions to complex scientific applications in structural chemistry, molecular biology, and nuclear fusion, specifically selected to assess surrogate model performance under conditions of *high dimensionality, severe multi-modality, and heterogeneous landscapes*—scenarios where standard stationary GPs typically flounder.

**Competing Methods** We compare RAMBO against a diverse set of state-of-the-art algorithms, beginning with *Standard Single-GP BO (SGP)* (Snoek et al., 2012); to ensure a fair comparison and isolate the impact of our regime-adaptive mechanism, we employ the standard Squared Exponential kernel for both the SGP baseline and RAMBO. To assess performance in high-dimensional and heterogeneous settings, we include *TuRBO*<sup>1</sup> (Eriksson et al., 2019), which restricts optimization to local trust regions to handle non-stationarity; *SAASBO*<sup>2</sup> (Eriksson and Jankowiak, 2021), which addresses high dimensionality via sparse axis-aligned subspace priors; *BAXUS*<sup>3</sup> (Papenmeier et al., 2022), which progressively expands

1. <https://github.com/uber-research/TuRBO>  
 2. <https://github.com/martinjankowiak/saasbo>  
 3. <https://github.com/lpapenme/BAXUS>

the dimensionality of its adaptive subspace embeddings; and *ALEBO*<sup>4</sup> (Letham et al., 2020), which optimizes within a linear embedding of the input space. Our evaluation also incorporates *HEBO*<sup>5</sup> (Cowen-Rivers et al., 2022), a robust method combining heteroscedastic GPs with input warping; *Bounce*<sup>6</sup> (Papenmeier et al., 2023), a trust-region approach designed for high-dimensional mixed spaces; *SMAC*<sup>7</sup> (Hutter et al., 2011), a random-forest-based alternative for non-smooth landscapes; and *COMBO*<sup>8</sup> (Oh et al., 2019), which utilizes graph kernels to model combinatorial variables. *Note that COMBO is omitted from the Drug Discovery and ConStellaration experiments because its computational complexity renders it intractable on these large-scale benchmarks.*

**Metrics and Experiment Settings** We report the *best objective value found so far* averaged over 5 independent seeds, with shaded regions denoting the *standard error*. All methods are initialized with (20 for synthetic and 5 for scientific design) identical quasirandom Sobol points. To ensure numerical stability, input features are normalized to the hypercube  $[-1, 1]^d$ , and target values are standardized (zero mean, unit variance) prior to model fitting in each iteration. RAMBO and the SGP baseline are implemented in PyTorch (Paszke et al., 2019), utilizing the *Expected Improvement (EI)* acquisition function. We optimize the acquisition function using L-BFGS with 20 *random restarts*, selecting the candidate with the highest acquisition value to update the dataset. For RAMBO, cluster-specific kernel parameters are optimized via Adam by maximizing the marginal log likelihood; inference is performed using collapsed Gibbs sampling with a burn-in of 500 iterations. Other baselines use their official implementations; all experiments except SAASBO ran on CPU-only resources.

## 6.1 Synthetic Benchmarks

We validate RAMBO on two canonical test functions designed to stress-test optimization in pathological multi-modal landscapes. The *Levy function*<sup>9</sup> is characterized by a rugged surface with dense clusters of local minima, challenging the model’s ability to resolve fine-grained structures and navigate high-frequency oscillations. In contrast, the *Schwefel function*<sup>10</sup> presents a deceptive topology where the global optimum is geometrically isolated at the domain boundary, far removed from other local basins; this penalizes methods that over-exploit central regions. Formal definitions and visualizations are provided in Appendix C.1 and C.2. We evaluate performance across varying dimensions  $d \in \{6, 10\}$  to assess scalability across distinct regimes: from low-dimensional settings that allow for visual verification of regime discovery, to high-dimensional spaces where standard stationary GPs typically falter. As shown in Figure 1a-1d, RAMBO with adaptive  $\alpha$ -scheduling (DPMM-Sched) consistently matches or outperforms all baselines across both functions and dimensionalities. On the Levy function, RAMBO converges to near-optimal values significantly faster than competing methods, while on the deceptive Schwefel landscape, the performance gap widens

---

4. <https://github.com/facebookresearch/alebo>

5. <https://github.com/huawei-noah/HEBO>

6. <https://github.com/lpapenme/bounce>

7. <https://github.com/automl/SMAC3>

8. <https://github.com/QUVA-Lab/COMBO>

9. <https://www.sfu.ca/~ssurjano/levy.html>

10. <https://www.sfu.ca/~ssurjano/schwef.html>

substantially—particularly in 10D, where stationary methods struggle to escape suboptimal basins. Notably, the scheduled  $\alpha$  variant outperforms fixed- $\alpha$  configurations, validating the benefit of adaptive regime discovery.

## 6.2 Real-World Scientific Design

**Molecular Conformer Optimization (12D)** Molecules continuously explore conformational space through rotations around single bonds (Hawkins et al., 2010; Riniker and Landrum, 2015). This benchmark involves finding the lowest-energy configuration of a linear alkane chain (pentadecane,  $C_{15}H_{32}$ ) by optimizing  $d = 12$  internal dihedral angles using force field calculations (Halgren, 1996; Grimme et al., 2017). Rotation around each C–C bond favors three orientations— $180^\circ$  (anti) and  $\pm 60^\circ$  (gauche)—inducing a combinatorial explosion of locally stable states. With  $3^{12} = 531,441$  potential conformational minima separated by high-energy steric barriers, the landscape is highly multimodal with sharp transitions between basins. A detailed problem description is provided in Appendix C.3. Figure 1e demonstrates that RAMBO substantially outperforms all baselines on this 12D conformational landscape. After 200 iterations, RAMBO achieves an energy 8.05 kcal/mol, compared to 13.36 kcal/mol for the best baseline (SAASBO), representing a 39.73% improvement. Most competing methods stagnate at high-energy local minima, whereas RAMBO—particularly with adaptive  $\alpha$ -scheduling—efficiently navigates between distinct rotameric basins to reach near-optimal configurations within 50 iterations.

**Virtual Screening for Drug Discovery (50D)** We optimize small molecules for docking scores against a cancer-related protein target (PDB ID: 6T2W). The inputs are 2048-bit Morgan fingerprints (Rogers and Hahn, 2010) compressed into a  $d = 50$  dimensional continuous latent space via Principal Component Analysis (PCA). This benchmark is representative of modern drug discovery pipelines (Gómez-Bombarelli et al., 2018; Griffiths and Hernández-Lobato, 2020; Korovina et al., 2020; Stanton et al., 2022; Liu et al., 2023; ?). This benchmark poses two key challenges: high dimensionality and the inherently disjoint nature of chemical space—distinct molecular scaffolds (e.g., different ring systems or functional groups) occupy separate regions in the latent space with fundamentally different structure-activity relationships (SAR). A detailed problem description is provided in Appendix C.4. As shown in Figure 1f, RAMBO substantially outperforms baselines in this 50D drug discovery task. By iteration 500, RAMBO achieves a docking score of -13.31, compared to -12.79 for the next-best method (TuRBO), representing a 4.06% improvement in predicted binding affinity. The mixture model’s ability to partition chemical space into scaffold-specific regimes enables continued improvement throughout the 500-iteration budget, while single-surrogate methods stagnate in early iterations.

**Nuclear Fusion Reactor (81D)** This benchmark optimizes the shape of a stellarator fusion reactor to maximize quasi-isodynamic quality, a measure of particle confinement efficiency (Gates et al., 2018; Cadena et al., 2025). The inputs are Fourier coefficients controlling the plasma boundary geometry. Stellarator design exhibits highly nonlinear physics: small perturbations in boundary shape can trigger abrupt transitions in magnetic field topology and plasma stability, creating a patchy landscape where regions of high confinement quality are interspersed with unstable configurations. A detailed problem description is

provided in Appendix C.5. Figure 1g shows that RAMBO achieves substantially higher confinement quality than all baselines, reaching  $Q_i$  values approximately 51.55% higher than the best competing method. RAMBO discovers 3-5 regimes corresponding to distinct magnetic topologies, modeling configurations near nested flux surfaces separately from those approaching island formation. Stable high- $Q_i$  regions receive moderate length scales, while boundary regions near instabilities are modeled with shorter length scales to capture rapid quality degradation. Embedding-based methods (ALEBO, SAASBO) struggle because stellarator physics involves dense interactions among Fourier coefficients, violating both the low-rank linear structure assumed by ALEBO and the axis-aligned sparsity assumed by SAASBO. Trust-region methods (TuRBO) plateau when the local region straddles a stability boundary. RAMBO’s regime-aware surrogates avoid these failure modes, enabling continued improvement throughout the 500-iteration budget.

## 7. Conclusion

We presented RAMBO, a regime-adaptive Bayesian optimization framework that replaces the standard stationary GP surrogate with a Dirichlet Process Mixture of Gaussian Processes. By automatically discovering and modeling distinct regimes with locally-optimized hyperparameters, RAMBO captures the discrete heterogeneity prevalent in scientific design problems—where continuous non-stationary kernels fall short. Our collapsed Gibbs sampling procedure enables efficient inference, while adaptive  $\alpha$ -scheduling balances model parsimony against expressive power as data accumulates. Experiments across synthetic benchmarks and real-world applications in molecular conformation, drug discovery, and fusion reactor design demonstrate consistent improvements over state-of-the-art baselines.

## References

Charles E Antoniak. Mixtures of Dirichlet processes with applications to Bayesian nonparametric problems. *The Annals of Statistics*, 2(6):1152–1174, 1974.

Peter Auer, Nicolò Cesa-Bianchi, and Paul Fischer. Finite-time analysis of the multiarmed bandit problem. *Machine Learning*, 47(2):235–256, 2002.

James Bergstra, Rémi Bardenet, Yoshua Bengio, and Balázs Kégl. Algorithms for hyperparameter optimization. In *Advances in Neural Information Processing Systems*, volume 24, pages 2546–2554, 2011.

Eric Brochu, Vlad M Cora, and Nando de Freitas. A tutorial on Bayesian optimization of expensive cost functions, with application to active user modeling and hierarchical reinforcement learning. *arXiv preprint arXiv:1012.2599*, 2010.

Santiago A Cadena, Andrea Merlo, Emanuel Laude, Alexander Bauer, Atul Agrawal, Maria Pascu, Marija Savtchouk, Enrico Guiraud, Lukas Bonauer, Stuart Hudson, and Markus Kaiser. ConStellaration: A dataset of QI-like stellarator plasma boundaries and optimization benchmarks. In *Advances in Neural Information Processing Systems*, 2025. URL <https://openreview.net/forum?id=NQSBGK1Cpx>.

Sayak Ray Chowdhury and Aditya Gopalan. On kernelized multi-armed bandits. In *Proceedings of the 34 th International Conference on Machine Learning*, pages 844–853. PMLR, 2017.

Alexander I Cowen-Rivers, Wenlong Lyu, Rasul Tutunov, Zhi Wang, Antoine Grosnit, Ryan Rhys Griffiths, Alexandre Max Maraval, Hao Jianye, Jun Wang, Jan Peters, and Haitham Bou-Ammar. HEBO: Pushing the limits of sample-efficient hyperparameter optimisation. *Journal of Artificial Intelligence Research*, 74:1269–1349, 2022.

Andreas C Damianou and Neil D Lawrence. Deep Gaussian processes. In *Proceedings of the Sixteenth International Conference on Artificial Intelligence and Statistics*, pages 207–215. JMLR.org, 2013.

Aryan Deshwal and Janardhan Rao Doppa. Combining latent space and structured kernels for Bayesian optimization over combinatorial spaces. In *Advances in Neural Information Processing Systems*, volume 34, pages 8185–8200, 2021.

Thomas Elsken, Jan Hendrik Metzen, and Frank Hutter. Neural architecture search: A survey. *Journal of Machine Learning Research*, 20(55):1–21, 2019.

David Eriksson and Martin Jankowiak. High-dimensional Bayesian optimization with sparse axis-aligned subspaces. In *Proceedings of the Thirty-Seventh Conference on Uncertainty in Artificial Intelligence*, pages 493–503. AUAI Press, 2021.

David Eriksson and Matthias Poloczek. Scalable constrained Bayesian optimization. In *Proceedings of the 24th International Conference on Artificial Intelligence and Statistics*, pages 730–738. PMLR, 2021.

David Eriksson, Michael Pearce, Jacob R Gardner, Ryan Turner, and Matthias Poloczek. Scalable global optimization via local Bayesian optimization. In *Advances in Neural Information Processing Systems*, volume 32, pages 5497–5508, 2019.

Michael D Escobar and Mike West. Bayesian density estimation and inference using mixtures. *Journal of the American Statistical Association*, 90(430):577–588, 1995.

Stefan Falkner, Aaron Klein, and Frank Hutter. BOHB: Robust and efficient hyperparameter optimization at scale. In *Proceedings of the 35th International Conference on Machine Learning*, pages 1437–1446. PMLR, 2018.

Thomas S Ferguson. A Bayesian analysis of some nonparametric problems. *The Annals of Statistics*, 1(2):209–230, 1973.

Matthias Feurer and Frank Hutter. Automated machine learning. *Cham: Springer*, pages 113–134, 2019.

Peter Frazier, Warren Powell, and Savas Dayanik. The knowledge-gradient policy for correlated normal beliefs. *INFORMS Journal on Computing*, 21(4):599–613, 2009.

Peter I Frazier. A tutorial on bayesian optimization. *arXiv preprint arXiv:1807.02811*, 2018.

Eduardo C Garrido-Merchán and Daniel Hernández-Lobato. Dealing with categorical and integer-valued variables in Bayesian optimization with Gaussian processes. *Neurocomputing*, 380:20–35, 2020.

David A Gates, David Anderson, S Anderson, M Zarnstorff, Donald A Spong, Harold Weitzner, G H Neilson, D Ruzic, D Andruczyk, J H Harris, H Mynick, C C Hegna, O Schmitz, J N Talmadge, D Curreli, D Maurer, A H Boozer, S Knowlton, J P Allain, D Ennis, G Wurden, A Reiman, J D Lore, Matt Landreman, J P Freidberg, S R Hudson, M Porkolab, D Demers, J Terry, E Edlund, S A Lazerson, N Pablant, R Fonck, F Volpe, J Canik, R Granetz, A Ware, J D Hanson, S Kumar, C Deng, K Likin, A Cerfon, A Ram, A Hassam, S Prager, C Paz-Soldan, M J Pueschel, I Joseph, and A. H Glasser. Stellarator research opportunities: A report of the national stellarator coordinating committee. *Journal of Fusion Energy*, 37(1):51–94, 2018.

Andrew Gelman, John B Carlin, Hal S Stern, David B Dunson, Aki Vehtari, and Donald B Rubin. *Bayesian Data Analysis*. CRC Press, third edition, 2013.

Marc G Genton. Classes of kernels for machine learning: a statistics perspective. *Journal of Machine Learning Research*, 2:299–312, 2001.

Frederick W Goldberg, M Raymond V Finlay, Attilla K T Ting, David Beattie, Gillian M Lamont, Charlene Fallan, Gail L Wrigley, Marianne Schimpl, Martin R Howard, Beth Williamson, Mercedes Vazquez-Chantada, Derek G Barratt, Barry R Davies, Elaine B Cadogan, Antonio Ramos-Montoya, and Emma Dean. The discovery of 7-methyl-2-[(7-methyl[1,2,4]triazolo[1,5-a]pyridin-6-yl)amino]-9-(tetrahydro-2H-pyran-4-yl)-7,9-dihydro-8H-purin-8-one (AZD7648), a potent and selective DNA-dependent protein kinase (DNA-PK) inhibitor. *Journal of Medicinal Chemistry*, 63(7):3461–3471, 2020.

Rafael Gómez-Bombarelli, Jennifer N Wei, David Duvenaud, José Miguel Hernández-Lobato, Benjamín Sánchez-Lengeling, Dennis Sheberla, Jorge Aguilera-Iparraguirre, Timothy D Hirzel, Ryan P Adams, and Alán Aspuru-Guzik. Automatic chemical design using a data-driven continuous representation of molecules. *ACS Central Science*, 4(2):268–276, 2018.

A G Goodman, K Camacho Mata, S A Henneberg, R Jorge, M Landreman, G G Plunk, H M Smith, R J J Mackenbach, C D Beidler, and P Helander. Constructing precisely quasi-isodynamic magnetic fields. *Journal of Plasma Physics*, 89(5):905890504, 2023.

Robert B Gramacy and Herbert K H Lee. Bayesian treed Gaussian process models with an application to computer modeling. *Journal of the American Statistical Association*, 103 (483):1119–1130, 2008.

Ryan-Rhys Griffiths and José Miguel Hernández-Lobato. Constrained Bayesian optimization for automatic chemical design using variational autoencoders. *Chemical Science*, 11(2): 577–586, 2020.

Stefan Grimme, Christoph Bannwarth, and Philip Shushkov. A robust and accurate tight-binding quantum chemical method for structures, vibrational frequencies, and noncovalent

interactions of large molecular systems parametrized for all spd-block elements ( $Z=1-86$ ). *Journal of Chemical Theory and Computation*, 13(5):1989–2009, 2017.

Thomas A Halgren. Merck molecular force field. I. Basis, form, scope, parameterization, and performance of MMFF94. *Journal of Computational Chemistry*, 17(5-6):490–519, 1996.

W Keith Hastings. Monte Carlo sampling methods using Markov chains and their applications. *Biometrika*, 57(1):97–109, 1970.

Paul C D Hawkins, A Geoffrey Skillman, Gregory L Warren, Benjamin A Ellingson, and Matthew T Stahl. Conformer generation with OMEGA: algorithm and validation using high quality structures from the Protein Databank and Cambridge Structural Database. *Journal of Chemical Information and Modeling*, 50(4):572–584, 2010.

Harold Stanley Heaps. *Information retrieval: Computational and theoretical aspects*. Academic Press, Inc., 1978.

P Helander and J Nührenberg. Bootstrap current and neoclassical transport in quasi-isodynamic stellarators. *Plasma Physics and Controlled Fusion*, 51(5):055004, 2009.

Per Helander. Theory of plasma confinement in non-axisymmetric magnetic fields. *Reports on Progress in Physics*, 77(8):087001, 2014.

Philipp Hennig and Christian J Schuler. Entropy search for information-efficient global optimization. *Journal of Machine Learning Research*, 13:1809–1837, 2012.

José Miguel Hernández-Lobato, Matthew W Hoffman, and Zoubin Ghahramani. Predictive entropy search for efficient global optimization of black-box functions. In *Advances in Neural Information Processing Systems*, volume 27, pages 918–926, 2014.

Dave Higdon, Jenise Swall, and John Kern. Non-stationary spatial modeling. *Bayesian Statistics*, 6(1):761–768, 1999.

S. P. Hirshman and J. C. Whitson. Steepest-descent moment method for three-dimensional magnetohydrodynamic equilibria. *Physics of Fluids*, 26(12):3553–3568, 1983.

D Huang, T T Allen, W I Notz, and R A Miller. Sequential kriging optimization using multiple-fidelity evaluations. *Structural and Multidisciplinary Optimization*, 32(5):369–382, 2006.

Frank Hutter, Holger H Hoos, and Kevin Leyton-Brown. Sequential model-based optimization for general algorithm configuration. In *Learning and Intelligent Optimization*, pages 507–523. Springer, 2011.

Carl Hvarfner, Erik Orm Hellsten, and Luigi Nardi. Vanilla Bayesian optimization performs great in high dimensions. In *Proceedings of the 41st International Conference on Machine Learning*, pages 20793–20817. PMLR, 2024.

Hemant Ishwaran and Lancelot F James. Gibbs sampling methods for stick-breaking priors. *Journal of the American Statistical Association*, 96(453):161–173, 2001.

Donald R Jones, Matthias Schonlau, and William J Welch. Efficient global optimization of expensive black-box functions. *Journal of Global optimization*, 13(4):455–492, 1998.

Kirthevasan Kandasamy, Jeff Schneider, and Barnabás Póczos. High dimensional Bayesian optimisation and bandits via additive models. In *Proceedings of the 32nd International Conference on Machine Learning*, pages 295–304. PMLR, 2015.

Kirthevasan Kandasamy, Gautam Dasarathy, Junier B Oliva, Jeff Schneider, and Barnabás Póczos. Gaussian process bandit optimisation with multi-fidelity evaluations. In *Advances in Neural Information Processing Systems*, volume 29, pages 992–1000, 2016.

Kirthevasan Kandasamy, Willie Neiswanger, Jeff Schneider, Barnabás Póczos, and Eric P Xing. Neural architecture search with Bayesian optimisation and optimal transport. In *Advances in Neural Information Processing Systems*, volume 31, pages 2016–2025, 2018.

Diederik P Kingma and Jimmy Ba. Adam: A method for stochastic optimization. In *International Conference on Learning Representations*, 2015.

Ksenia Korovina, Sailun Xu, Kirthevasan Kandasamy, Willie Neiswanger, Barnabás Póczos, Jeff Schneider, and Eric P Xing. ChemBO: Bayesian optimization of small organic molecules with synthesizable recommendations. In *Proceedings of the Twenty Third International Conference on Artificial Intelligence and Statistics*, pages 3393–3403. PMLR, 2020.

H J Kushner. A new method of locating the maximum point of an arbitrary multipeak curve in the presence of noise. *Journal of Basic Engineering*, 86(1):97–106, 1964.

A Gilad Kusne, Heshan Yu, Changming Wu, Huairuo Zhang, Jason Hattrick-Simpers, Brian DeCost, Suchismita Sarker, Corey Oses, Cormac Toher, Stefano Curtarolo, Albert V Davydov, Ritesh Agarwal, Leonid A Bendersky, Mo Li, Apurva Mehta, and Ichiro Takeuchi. On-the-fly closed-loop materials discovery via Bayesian active learning. *Nature Communications*, 11(1):5966, 2020.

Greg Landrum et al. Rdkit: Open-source cheminformatics. <http://www.rdkit.org>, 2013. version 2025.09.3.

Benjamin Letham, Roberto Calandra, Akshara Rai, and Eytan Bakshy. Re-examining linear embeddings for high-dimensional Bayesian optimization. In *Advances in Neural Information Processing Systems*, volume 33, pages 1546–1558, 2020.

Shibo Li, Wei Xing, Robert M Kirby, and Shandian Zhe. Multi-fidelity Bayesian optimization via deep neural networks. In *Advances in Neural Information Processing Systems*, volume 33, pages 8521–8531, 2020.

Shibo Li, Robert Kirby, and Shandian Zhe. Batch multi-fidelity Bayesian optimization with deep auto-regressive networks. In *Advances in Neural Information Processing Systems*, volume 34, pages 25463–25475, 2021.

Jun S Liu. The collapsed Gibbs sampler in Bayesian computations with applications to a gene regulation problem. *Journal of the American Statistical Association*, 89(427):958–966, 1994.

Xuefeng Liu, Songhao Jiang, Archit Vasan, Alexander Brace, Ozan Gokdemir, Thomas Brettin, Fangfang Xia, Ian Foster, and Rick Stevens. DrugImprover: Utilizing reinforcement learning for multi-objective alignment in drug optimization. In *NeurIPS 2023 Workshop on New Frontiers of AI for Drug Discovery and Development*, 2023. URL <https://openreview.net/forum?id=8RPbt0C6S1>.

Turab Lookman, Prasanna V Balachandran, Dezhen Xue, and Ruihao Yuan. Active learning in materials science with emphasis on adaptive sampling using uncertainties for targeted design. *npj Computational Materials*, 5(1):21, 2019.

David JC MacKay et al. Introduction to gaussian processes. *NATO ASI series F computer and systems sciences*, 168:133–166, 1998.

Bertil Matérn. Spatial variation: Stochastic models and their application to some problems in forest surveys and other sampling investigations. *Meddelanden från Statens Skogsforskningsinstitut*, 49(5), 1960.

Mark McGann. FRED and HYBRID docking performance on standardized datasets. *Journal of computer-aided molecular design*, 26(8):897–906, 2012.

Geoffrey J McLachlan and David Peel. *Finite mixture models*. John Wiley and Sons, 2000.

Edward Meeds and Simon Osindero. An alternative infinite mixture of Gaussian process experts. In *Advances in Neural Information Processing Systems*, volume 18, pages 883–890, 2005.

Jonas Mockus. The application of bayesian methods for seeking the extremum. *Towards global optimization*, 2:117, 1998.

Radford M Neal. Markov chain sampling methods for Dirichlet process mixture models. *Journal of Computational and Graphical Statistics*, 9(2):249–265, 2000.

Trung Nguyen and Edwin Bonilla. Fast allocation of Gaussian process experts. In *Proceedings of the 31st International Conference on Machine Learning*, pages 145–153. PMLR, 2014.

ChangYong Oh, Jakub Tomczak, Efstratios Gavves, and Max Welling. Combinatorial Bayesian optimization using the graph Cartesian product. In *Advances in Neural Information Processing Systems*, volume 32, pages 2914–2924, 2019.

Christopher J Paciorek and Mark J Schervish. Nonstationary covariance functions for Gaussian process regression. In *Advances in Neural Information Processing Systems*, volume 16, pages 273–280, 2003.

Leonard Papenmeier, Luigi Nardi, and Matthias Poloczek. Increasing the scope as you learn: Adaptive Bayesian optimization in nested subspaces. In *Advances in Neural Information Processing Systems*, volume 35, pages 11586–11601, 2022.

Leonard Papenmeier, Luigi Nardi, and Matthias Poloczek. Bounce: Reliable high-dimensional Bayesian optimization for combinatorial and mixed spaces. In *Advances in Neural Information Processing Systems*, volume 36, pages 1764–1793, 2023.

Adam Paszke, Sam Gross, Francisco Massa, Adam Lerer, James Bradbury, Gregory Chanan, Trevor Killeen, Zeming Lin, Natalia Gimelshein, Luca Antiga, Alban Desmaison, Andreas Kopf, Edward Yang, Zach DeVito, Martin Raison, Alykhan Tejani, Sasank Chilamkurthy, Benoit Steiner, Lu Fang, Junjie Bai, and Soumith Chintala. PyTorch: An imperative style, high-performance deep learning library. In *Advances in Neural Information Processing Systems*, volume 32, pages 8026–8037, 2019.

Jim Pitman and Marc Yor. The two-parameter Poisson-Dirichlet distribution derived from a stable subordinator. *The Annals of Probability*, 25(2):855–900, 1997.

Christian Plagemann, Kristian Kersting, and Wolfram Burgard. Nonstationary gaussian process regression using point estimates of local smoothness. In *Joint European Conference on Machine Learning and Knowledge Discovery in Databases*, pages 204–219. Springer, 2008.

Matthias Poloczek, Jialei Wang, and Peter I Frazier. Multi-information source optimization. In *Advances in Neural Information Processing Systems*, volume 30, pages 4288–4298, 2017.

Carl Edward Rasmussen. *Gaussian processes in machine learning*. Springer, 2003.

Carl Edward Rasmussen and Zoubin Ghahramani. Infinite mixtures of Gaussian process experts. In *Advances in Neural Information Processing Systems*, volume 14, pages 881–888, 2001.

Sereina Riniker and Gregory A Landrum. Better informed distance geometry: using what we know to improve conformation generation. *Journal of Chemical Information and Modeling*, 55(12):2562–2574, 2015.

David Rogers and Mathew Hahn. Extended-connectivity fingerprints. *Journal of Chemical Information and Modeling*, 50(5):742–754, 2010.

Binxin Ru, Ahsan S Alvi, Vu Nguyen, Michael A Osborne, and Stephen J Roberts. Bayesian optimisation over multiple continuous and categorical inputs. In *Proceedings of the 37th International Conference on Machine Learning*, pages 8276–8285. PMLR, 2020.

Daniel J Russo, Benjamin Van Roy, Abbas Kazerouni, Ian Osband, and Zheng Wen. A tutorial on Thompson sampling. *Foundations and Trends in Machine Learning*, 11(1):1–96, 2018.

Benjamin Sanchez-Lengeling and Alán Aspuru-Guzik. Inverse molecular design using machine learning: Generative models for matter engineering. *Science*, 361(6400):360–365, 2018.

Jonathan Scarlett, Ilija Bogunovic, and Volkan Cevher. Lower bounds on regret for noisy Gaussian process bandit optimization. In *Proceedings of the 2017 Conference on Learning Theory*, pages 1723–1742. PMLR, 2017.

Bernhard Schölkopf and Alexander J Smola. *Learning with Kernels: Support Vector Machines, Regularization, Optimization, and Beyond*. MIT Press, 2002.

Jayaram Sethuraman. A constructive definition of Dirichlet priors. *Statistica Sinica*, 4(2): 639–650, 1994.

Bobak Shahriari, Kevin Swersky, Ziyu Wang, Ryan P Adams, and Nando de Freitas. Taking the human out of the loop: A review of Bayesian optimization. *Proceedings of the IEEE*, 104(1):148–175, 2016.

Jasper Snoek, Hugo Larochelle, and Ryan P Adams. Practical Bayesian optimization of machine learning algorithms. In *Advances in Neural Information Processing Systems*, volume 25, pages 2951–2959, 2012.

Jasper Snoek, Kevin Swersky, Rich Zemel, and Ryan Adams. Input warping for bayesian optimization of non-stationary functions. In *International conference on machine learning*, pages 1674–1682. PMLR, 2014.

Jasper Snoek, Oren Rippel, Kevin Swersky, Ryan Kiros, Nadathur Satish, Narayanan Sundaram, Md. Mostafa Ali Patwary, Prabhat, and Ryan P. Adams. Scalable Bayesian optimization using deep neural networks. In *Proceedings of the 32nd International Conference on Machine Learning*, pages 2171–2180. PMLR, 2015.

Jost Tobias Springenberg, Aaron Klein, Stefan Falkner, and Frank Hutter. Bayesian optimization with robust Bayesian neural networks. In *Advances in Neural Information Processing Systems*, volume 29, pages 4134–4142, 2016.

Niranjan Srinivas, Andreas Krause, Sham M Kakade, and Matthias Seeger. Gaussian process optimization in the bandit setting: No regret and experimental design. *arXiv preprint arXiv:0912.3995*, 2009.

Niranjan Srinivas, Andreas Krause, Sham Kakade, and Seeger Matthias. Gaussian process optimization in the bandit setting: No regret and experimental design. In *Proceedings of the 27th International Conference on Machine Learning*, pages 1015–1022, 2010.

Samuel Stanton, Wesley Maddox, Nate Gruber, Philip Maffettone, Emily Delaney, Peyton Greenside, and Andrew Gordon Wilson. Accelerating Bayesian optimization for biological sequence design with denoising autoencoders. In *Proceedings of the 39th International Conference on Machine Learning*, pages 20459–20478. PMLR, 2022.

Teague Sterling and John J Irwin. ZINC 15 – ligand discovery for everyone. *Journal of Chemical Information and Modeling*, 55(11):2324–2337, 2015.

Shion Takeno, Hitoshi Fukuoka, Yuhki Tsukada, Toshiyuki Koyama, Motoki Shiga, Ichiro Takeuchi, and Masayuki Karasuyama. Multi-fidelity Bayesian optimization with max-value entropy search and its parallelization. In *Proceedings of the 37th International Conference on Machine Learning*, pages 9334–9345. PMLR, 2020.

William D Tap, Zev A Wainberg, Stephen P Anthony, Prabha N Ibrahim, Chao Zhang, John H Healey, Bartosz Chmielowski, Arthur P Staddon, Allen Lee Cohn, Geoffrey I Shapiro, et al. Structure-guided blockade of CSF1R kinase in tenosynovial giant-cell tumor. *New England Journal of Medicine*, 373(5):428–437, 2015.

William R Thompson. On the likelihood that one unknown probability exceeds another in view of the evidence of two samples. *Biometrika*, 25(3/4):285–294, 1933.

Volker Tresp. Mixtures of Gaussian processes. In *Advances in Neural Information Processing Systems*, volume 13, pages 654–660, 2000.

Xingchen Wan, Vu Nguyen, Huong Ha, Binxin Ru, Cong Lu, and Michael A Osborne. Think global and act local: Bayesian optimisation over high-dimensional categorical and mixed search spaces. In *Proceedings of the 38th International Conference on Machine Learning*, pages 10663–10674. PMLR, 2021.

Zi Wang and Stefanie Jegelka. Max-value entropy search for efficient Bayesian optimization. In *International Conference on Machine Learning*, pages 3627–3635. PMLR, 2017.

Ziyu Wang, Frank Hutter, Masrour Zoghi, David Matheson, and Nando de Freitas. Bayesian optimization in a billion dimensions via random embeddings. *Journal of Artificial Intelligence Research*, 55:361–387, 2016.

Jiachen Wen, Siyuan Wang, Rongxian Guo, and Dan Liu. Csf1r inhibitors are emerging immunotherapeutic drugs for cancer treatment. *European Journal of Medicinal Chemistry*, 245:114884, 2023.

Colin White, Willie Neiswanger, and Yash Savani. BANANAS: Bayesian optimization with neural architectures for neural architecture search. In *Proceedings of the Thirty-Fifth AAAI Conference on Artificial Intelligence*, pages 10293–10301. AAAI Press, 2021.

Christopher K. I. Williams and Carl Edward Rasmussen. Gaussian processes for regression. In *Advances in Neural Information Processing Systems*, volume 8, pages 514–520. MIT Press, 1995.

Andrew Gordon Wilson, Zhiting Hu, Ruslan Salakhutdinov, and Eric P Xing. Deep kernel learning. In *Artificial intelligence and statistics*, pages 370–378. PMLR, 2016a.

Andrew Gordon Wilson, Zhiting Hu, Ruslan Salakhutdinov, and Eric P Xing. Stochastic variational deep kernel learning. In *Advances in Neural Information Processing Systems*, volume 29, pages 2586–2594, 2016b.

James Wilson, Frank Hutter, and Marc Deisenroth. Maximizing acquisition functions for Bayesian optimization. In *Advances in Neural Information Processing Systems*, volume 31, pages 9884–9895, 2018.

Jian Wu and Peter I. Frazier. The parallel knowledge gradient method for batch Bayesian optimization. In *Advances in Neural Information Processing Systems*, volume 29, pages 3126–3134. Curran Associates, Inc., 2016.

Zhitong Xu, Haitao Wang, Jeff M Phillips, and Shandian Zhe. Standard Gaussian process is all you need for high-dimensional Bayesian optimization. In *The Thirteenth International Conference on Learning Representations*, 2025. URL <https://openreview.net/forum?id=kX8h23UG6v>.

Dezhen Xue, Prasanna V Balachandran, John Hogden, James Theiler, Deqing Xue, and Turab Lookman. Accelerated search for materials with targeted properties by adaptive design. *Nature Communications*, 7(1):11241, 2016.

Chao Yuan and Claus Neubauer. Variational mixture of Gaussian process experts. In *Advances in Neural Information Processing Systems*, volume 21, pages 1897–1904, 2008.

Barret Zoph and Quoc V Le. Neural architecture search with reinforcement learning. In *International Conference on Learning Representations*, 2017. URL <https://openreview.net/forum?id=r1Ue8Hcxg>.

## Appendix A. Extended Acquisition Functions

In this section, we provide the detailed derivations for the Max-value Entropy Search (MES) and Probability of Improvement (PI) acquisition functions within the RAMBO framework. Both derivations address the challenge of the multimodal posterior predictive distribution inherent to the DPMM-GP.

### A.1 Max-value Entropy Search (MES)

We extend the Max-value Entropy Search (MES) (Wang and Jegelka, 2017) to the DPMM-GP framework. MES seeks to evaluate the candidate point  $x$  that maximizes the mutual information between the observation  $y$  at  $x$  and the global maximum value  $y^* = \max_{x' \in \mathcal{X}} f(x')$ .

The acquisition function is defined as the expected reduction in the entropy of the predictive distribution  $p(y|x)$  induced by the knowledge of the global maximum  $y^*$ :

$$\alpha_{MES}(x) = I(y; y^*) = H(y|x) - \mathbb{E}_{y^*} [H(y | x, y < y^*)] \quad (16)$$

where the expectation is taken over the posterior distribution of the global maximum  $p(y^*|\mathcal{D})$ . Due to the multimodal nature of the DPMM-GP posterior, neither term has a closed analytical form. We derive tractable approximations for both below.

**Entropy of the Predictive Mixture** The predictive distribution  $p(y|x)$  is a Gaussian Mixture Model (GMM) with weights  $w_k(x)$  and component parameters  $\{\mu_{*,k}(x), \sigma_{*,k}^2(x)\}$  (Theorem 3.3). As the entropy of a GMM does not have a closed-form expression, we approximate it via *moment matching*. We treat the entropy of the mixture as the entropy of a single Gaussian with the equivalent variance  $\sigma_{mix}^2(x)$  derived in Theorem 3.4:

$$H(y|x) \approx \frac{1}{2} \log (2\pi e \sigma_{mix}^2(x)). \quad (17)$$

This provides a coherent upper bound on the true entropy, as the Gaussian distribution maximizes entropy for a fixed variance.

**Expected Conditional Entropy** The second term requires computing the entropy of the predictive distribution truncated at  $y^*$ , averaged over samples of  $y^*$ . We approximate the distribution  $p(y^*)$  via Monte Carlo sampling. To draw a sample  $y_s^*$ , we use a two-stage ancestral sampling procedure consistent with our generative model:

1. **Regime Selection:** Sample a latent regime index  $k \sim \text{Categorical}(\pi)$ , where  $\pi$  represents the global cluster weights.
2. **Function Maximization:** Draw a sample from the global maximum of the  $k$ -th GP component. Following standard practice, we approximate this via a Gumbel distribution sample based on the discrete maximum of the GP on the training data.

Given a sample  $y_s^*$ , the conditional distribution  $p(y|x, y < y_s^*)$  is a truncated GMM. We approximate its entropy as the probabilistically weighted sum of the entropies of its truncated Gaussian components. Let  $\gamma_{k,s} = \frac{y_s^* - \mu_{*,k}(x)}{\sigma_{*,k}(x)}$  be the standardized distance to the maximum for regime  $k$ . The entropy of the  $k$ -th Gaussian component truncated at  $y_s^*$  is:

$$H_k(y|y < y_s^*) = \frac{1}{2} \log(2\pi e \sigma_{*,k}^2) + \ln \Phi(\gamma_{k,s}) - \frac{1}{2} \frac{\gamma_{k,s} \phi(\gamma_{k,s})}{\Phi(\gamma_{k,s})}. \quad (18)$$

Substituting this into Eq. (16) and simplifying (noting that the constant variance terms cancel out in the differential information gain formulation), we arrive at the numerical estimator:

$$\alpha_{MES}(x) \approx \frac{1}{S} \sum_{s=1}^S \sum_{k=1}^{K+1} w_k(x) \left[ \frac{\gamma_{k,s} \phi(\gamma_{k,s})}{2\Phi(\gamma_{k,s})} - \ln \Phi(\gamma_{k,s}) \right] \quad (19)$$

where  $S$  is the number of Monte Carlo samples for  $y^*$ , and  $\phi, \Phi$  are the standard normal PDF and CDF, respectively.

## A.2 Probability of Improvement (PI)

We extend the Probability of Improvement (PI) strategy (Kushner, 1964) to the DPMM-GP framework. Standard PI seeks to maximize the probability that the function value at a candidate point  $x$  exceeds the current best observation  $f^+$  by some margin  $\xi \geq 0$ .

In the context of our mixture model, the predictive distribution is multimodal. Consequently, the probability of improvement is not merely a function of a single mean and variance, but a weighted combination of the improvement probabilities offered by each latent regime.

**Theorem 10 (DPMM-GP Probability of Improvement)** *Let  $f^+$  denote the current best observed value, and let  $\xi \geq 0$  be a user-specified exploration parameter. The Probability of Improvement at input  $x$  under the DPMM-GP posterior is the probability-weighted sum of the PI values for each constituent GP component:*

$$\alpha_{PI}(x) = \sum_{k=1}^{K+1} w_k(x) \cdot \Phi \left( \frac{\mu_{*,k}(x) - f^+ - \xi}{\sigma_{*,k}(x)} \right) \quad (20)$$

where  $w_k(x) \approx p(z_* = k | x, \mathcal{D})$  are the gating weights defined in Eq. (8), and  $(\mu_{*,k}(x), \sigma_{*,k}(x))$  are the posterior mean and standard deviation of the  $k$ -th GP regime.

**Proof** The acquisition function  $\alpha_{PI}(x)$  is defined as the probability that the latent function value  $f(x)$  exceeds the target  $f^+ + \xi$ :

$$\alpha_{PI}(x) = \mathbb{P}[f(x) > f^+ + \xi]. \quad (21)$$

We proceed by marginalizing over the latent regime assignments  $z_*$  for the test point  $x$ . Using the Law of Total Probability:

$$\mathbb{P}[f(x) > f^+ + \xi] = \sum_{k=1}^{K+1} \mathbb{P}[f(x) > f^+ + \xi | z_* = k] \cdot p(z_* = k | x, \mathcal{D}). \quad (22)$$

From Theorem 3.3, the conditional distribution of  $f(x)$  given the assignment  $z_* = k$  is a Gaussian Process posterior:

$$p(f(x) | z_* = k) = \mathcal{N}(f(x) | \mu_{*,k}(x), \sigma_{*,k}^2(x)). \quad (23)$$

The conditional probability of improvement for this specific Gaussian component is given by the standard PI formula:

$$\mathbb{P}[f(x) > f^+ + \xi \mid z_* = k] = \int_{f^+ + \xi}^{\infty} \mathcal{N}(f \mid \mu_{*,k}(x), \sigma_{*,k}^2(x)) df \quad (24)$$

$$= \Phi\left(\frac{\mu_{*,k}(x) - (f^+ + \xi)}{\sigma_{*,k}(x)}\right). \quad (25)$$

Substituting the mixture weights  $w_k(x)$  for  $p(z_* = k \mid x, \mathcal{D})$  and the component probabilities back into the total probability sum yields Eq. (20).  $\blacksquare$

### A.3 Upper Confidence Bound (UCB)

The Upper Confidence Bound (UCB) acquisition function (Srinivas et al., 2009) is widely used for its explicit management of the exploration-exploitation trade-off. Standard UCB is defined for a single Gaussian posterior; however, it extends naturally to the DPMM-GP by utilizing the mixture moments derived in Theorem 3.4.

Given the posterior predictive mixture with mean  $\mu_{mix}(x)$  and variance  $\sigma_{mix}^2(x)$ , the Mixture UCB acquisition function is defined as:

$$\alpha_{UCB}(x) = \mu_{mix}(x) + \sqrt{\beta_t} \cdot \sigma_{mix}(x) \quad (26)$$

where  $\beta_t$  is a time-dependent confidence parameter. A key property of RAMBO is that the variance term  $\sigma_{mix}(x)$  encapsulates two distinct forms of uncertainty (Eq. 10):

- **Intra-regime uncertainty:** The average aleatoric variance of the individual GP experts ( $\sum w_k \sigma_{*,k}^2$ ).
- **Inter-regime disagreement:** The epistemic variance of the means across different regimes ( $\text{Var}_Z[\mu]$ ).

Consequently, Mixture UCB drives exploration not only where individual GPs are uncertain, but also where the regime assignment itself is ambiguous, naturally targeting regime boundaries for structural refinement.

### A.4 Thompson Sampling (TS)

Thompson Sampling (TS) (Thompson, 1933) is a randomized strategy that selects the next query point by optimizing a sample drawn from the posterior. It naturally handles the hierarchical structure of the DPMM-GP via ancestral sampling.

To select the next query point  $x_{new}$ , we perform the following two-stage procedure:

1. **Sample a Regime Assignment:** First, we sample a global regime index  $k$  from the current categorical weights of the mixture components:

$$\hat{z} \sim \text{Categorical}(\pi_1, \dots, \pi_K, \pi_{new}). \quad (27)$$

2. **Sample a Function Trajectory:** Conditioned on the chosen regime  $\hat{z}$ , we draw a continuous function realization  $\tilde{f}(\cdot)$  from the corresponding Gaussian Process posterior  $\mathcal{GP}(\mu_{*,\hat{z}}, \Sigma_{*,\hat{z}})$ . In practice, this is approximated efficiently using Random Fourier Features (RFF).
3. **Optimization:** The next query point is the global maximizer of the sampled function:

$$x_{new} = \arg \max_{x \in \mathcal{X}} \tilde{f}(x). \quad (28)$$

As  $t \rightarrow \infty$ , the posterior probability of the true regime approaches 1, and TS asymptotically recovers the behavior of optimizing the correct underlying expert.

### A.5 Knowledge Gradient (KG)

The Knowledge Gradient (KG) acquisition function (Frazier et al., 2009) quantifies the expected one-step improvement in the global maximum of the posterior predictive mean. Unlike EI, which measures improvement over the best *observation*, KG values the improvement in the *model's estimate* of the optimum.

Let  $\mu_n^* = \max_{x' \in \mathcal{X}} \mu_{mix,n}(x')$  denote the global maximum of the current mixture mean surface given dataset  $\mathcal{D}_n$ . If we were to effectively sample a candidate  $(x, y)$ , the dataset would evolve to  $\mathcal{D}_{n+1} = \mathcal{D}_n \cup \{(x, y)\}$ . This results in a new random posterior mean surface  $\mu_{mix,n+1}(\cdot)$ .

The KG acquisition value is defined as the expected increase in this surface maximum, marginalizing over the unknown outcome  $y$  and the latent regime assignment of the new point:

$$\alpha_{KG}(x) = \mathbb{E}_{y|x, \mathcal{D}_n} \left[ \max_{x' \in \mathcal{X}} \mu_{mix,n+1}(x' | x, y) - \mu_n^* \right]. \quad (29)$$

**Posterior Mean Update (The Fantasization Process)** Computing  $\mu_{mix,n+1}$  requires updating the DPMM-GP posterior with a "fantasy" observation  $(x, y)$ . In the exact inference limit, adding a point would require resampling all discrete regime assignments  $z_{1:n}$ . For computational tractability in the inner loop, we employ a *local update approximation*: we assume the assignments of the existing  $n$  points remain fixed, and we update the model based on the probabilistic assignment of the new point  $x$ .

The updated mixture mean at any test point  $x'$  is given by:

$$\mu_{mix,n+1}(x' | x, y) = \sum_{k=1}^{K+1} w_k^{(n+1)}(x') \cdot \mu_{*,k}^{(n+1)}(x'). \quad (30)$$

We compute the updated components as follows:

- **Component GP Update:** For each regime  $k$ , the GP posterior is updated conditioning on the event that  $(x, y)$  belongs to regime  $k$ . The updated mean function  $\mu_{*,k}^{(n+1)}(x')$  follows standard GP recursive equations:

$$\mu_{*,k}^{(n+1)}(x') = \mu_{*,k}^{(n)}(x') + \frac{k_k(x', x)}{k_k(x, x) + \sigma_{n,k}^2} (y - \mu_{*,k}^{(n)}(x)). \quad (31)$$

- **Gating Weight Update:** The mixture weights  $w_k(x')$  (Eq. 8) depend on the cluster counts  $n_k$  and the local predictive variance. The fantasy point  $(x, y)$  updates the effective count  $n_k$  by the probability that  $x$  belongs to  $k$ :  $\hat{\gamma}_k(x) \propto w_k^{(n)}(x) \cdot \mathcal{N}(y | \mu_{*,k}^{(n)}(x), \sigma_{*,k}^{2(n)}(x))$ . The updated weights  $w_k^{(n+1)}(x')$  are computed using the effective counts  $n_k + \hat{\gamma}_k(x)$ :

$$w_k^{(n+1)}(x') \propto \frac{n_k + \hat{\gamma}_k(x)}{n + 1 + \alpha} \cdot \exp\left(-\frac{1}{2} \log \sigma_{*,k}^{2(n+1)}(x')\right). \quad (32)$$

Since  $\mu_{mix,n+1}(x')$  is non-convex, we evaluate Eq. (29) via Monte Carlo integration with  $M$  fantasy samples drawn from the current posterior mixture  $y^{(m)} \sim \sum w_k(x) \mathcal{N}(\mu_{*,k}(x), \sigma_{*,k}^2(x))$ :

$$\alpha_{KG}(x) \approx \frac{1}{M} \sum_{m=1}^M \left( \max_{x' \in \mathcal{X}} \mu_{mix,n+1}(x' | x, y^{(m)}) - \mu_n^* \right). \quad (33)$$

The inner maximization is solved via multi-start L-BFGS, utilizing the updated gradients of the mixture mean.

## A.6 Predictive Entropy Search (PES)

Predictive Entropy Search (PES) (Hernández-Lobato et al., 2014) maximizes the mutual information between the observation  $y$  and the *location* of the global optimizer  $x^*$ .

$$\alpha_{PES}(x) = H(y | x, \mathcal{D}_n) - \mathbb{E}_{x^* | \mathcal{D}_n} [H(y | x, \mathcal{D}_n, x^*)]. \quad (34)$$

The first term is the entropy of the current posterior predictive mixture. As exact entropy for GMMs is intractable, we use the moment-matched Gaussian approximation (Theorem 3.4):

$$H(y | x, \mathcal{D}_n) \approx \frac{1}{2} \log (2\pi e \sigma_{mix}^2(x)). \quad (35)$$

The second term is the expected entropy of  $y$  conditioned on the constraint that  $x^*$  is the global maximizer. This constraint implies  $f(x^*) \geq f(x)$  for all  $x$ . We approximate this intractable expectation using a two-step procedure:

We draw samples of the global optimizer location utilizing the hierarchical generative process of the DPMM-GP. To generate a sample  $x_s^*$ :

- Sample a regime assignment  $\hat{z} \sim \text{Categorical}(\{w_k(x)\}_{k=1}^K)$ .
- Conditioned on  $\hat{z}$ , sample a function path  $\tilde{f} \sim \mathcal{GP}(\mu_{*,\hat{z}}, \Sigma_{*,\hat{z}})$  using Random Fourier Features (RFF) to ensure differentiability.
- Optimize the sampled path:  $x_s^* = \arg \max_{x \in \mathcal{X}} \tilde{f}(x)$ .

Conditioning on  $x_s^*$  imposes a complex set of gradient and value constraints on the random variable  $y(x)$ . For computational feasibility, we approximate the conditioning  $p(y | x, x_s^*)$  by the necessary condition  $y(x) < y(x_s^*) \approx \tilde{f}(x_s^*)$ . This effectively truncates the predictive distribution at the sampled maximum value  $f_{max}^s = \tilde{f}(x_s^*)$ .

The conditional entropy is approximated as the entropy of the mixture distribution truncated at  $f_{max}^s$ . For a single component  $k$ , the truncated variance  $v_k$  given an upper truncation point  $\beta$  is:

$$v_k(\beta) = \sigma_{*,k}^2(x) [1 - \delta_k(\beta)(\delta_k(\beta) + \alpha_k(\beta))] \quad (36)$$

where  $\alpha_k(\beta) = \frac{\beta - \mu_{*,k}(x)}{\sigma_{*,k}(x)}$  and  $\delta_k(\beta) = \frac{\phi(\alpha_k(\beta))}{\Phi(\alpha_k(\beta))}$ .

Aggregating over the mixture weights  $w_k(x)$ , the expected conditional entropy is approximated by:

$$\mathbb{E}_{x^*}[H(y|x, x^*)] \approx \frac{1}{S} \sum_{s=1}^S \frac{1}{2} \log \left( 2\pi e \sum_{k=1}^K w_k(x) v_k(f_{max}^s) \right). \quad (37)$$

This formulation directs sampling to regions where the outcome  $y$  would most significantly constrain the possible locations of  $x^*$ .

## Appendix B. Algorithms

### B.1 Collapsed Gibbs Sampler for DPMM-GP

Algorithm 1 presents the collapsed Gibbs sampler used for posterior inference in DPMM-GP. The key insight enabling efficient sampling is the analytical marginalization of latent function values  $\mathbf{f}$ , reducing the state space to only cluster assignments  $\mathbf{z}$  and hyperparameters  $\Theta$ .

The sampler iterates over each observation, temporarily removing it from its current cluster (lines 6–7) and computing reassignment probabilities. For existing clusters, the probability is proportional to the cluster size weighted by the GP predictive likelihood (line 8); for a new cluster, it is proportional to  $\alpha$  weighted by the prior predictive density under  $G_0$  (line 9). This follows directly from the Chinese Restaurant Process. After reassignment (lines 10–12), hyperparameters for each active cluster are updated either via Metropolis-Hastings or gradient ascent on the marginal likelihood (lines 14–15).

---

#### Algorithm 1 DPMM-GP Collapsed Gibbs Sampler

---

```

1: Input: Data  $\mathcal{D}$ , iterations  $T$ , conc.  $\alpha$ , base  $G_0$ 
2: Initialize  $z_i$  randomly for  $i = 1 \dots n$ 
3: Initialize  $\theta_k \sim G_0$  for initial clusters
4: for  $t = 1$  to  $T$  do
5:   for  $i = 1$  to  $n$  do
6:     Remove  $i$  from current cluster:  $n_{z_i} \leftarrow n_{z_i} - 1$ 
7:     If cluster empty, remove  $\theta_{z_i}$ 
8:     Compute probs for existing clusters:  $p_k \propto n_k \cdot \mathcal{N}(y_i \mid \mathcal{D}_k)$ 
9:     Compute prob for new cluster:  $p_{\text{new}} \propto \alpha \cdot p(y_i \mid G_0)$ 
10:    Sample  $z_i \sim \text{Categorical}(p_1, \dots, p_K, p_{\text{new}})$ 
11:    If  $z_i = \text{new}$ , draw  $\theta_{\text{new}} \sim p(\theta \mid y_i, G_0)$ 
12:    Add  $i$  to new cluster:  $n_{z_i} \leftarrow n_{z_i} + 1$ 
13:  end for
14:  for each active cluster  $k$  do
15:    Update  $\theta_k$  via MH or Gradient Ascent
16:  end for
17: end for

```

---

## B.2 Optimization Loop of RAMBO

RAMBO integrates the DPMM-GP surrogate with a sequential acquisition strategy, as outlined in Algorithm 2. The procedure begins by initializing 20 identical quasirandom Sobol points to ensure space-filling coverage. At each iteration, we perform collapsed Gibbs inference with warm starts from the previous assignments and hyperparameters to reduce burn-in overhead. The mixture Expected Improvement is then maximized via multi-start L-BFGS-B, initialized from uniform random samples, regime centroids, and perturbations around the current best solution. Finally, we update the dataset with the new observation and prune empty or low-weight regimes to maintain computational efficiency.

---

### Algorithm 2 RAMBO: Regime-Adaptive Mixture Bayesian Optimization

---

**Input:** Search space  $\mathcal{X}$ , budget  $T_{\max}$ , initial size  $n_{\text{init}}$

**Input:** Base concentration  $\alpha_0$ , MCMC samples  $S$ , restarts  $R$ , prune threshold  $\epsilon$

**Output:** Best solution  $\mathbf{x}^*$

```

1: // Phase 1: Initialization
2:  $\mathcal{D}_0 \leftarrow \text{SOBOL}(\mathcal{X}, n_{\text{init}})$ 
3: Initialize  $\Theta^{(0)}$  and  $\mathbf{z}^{(0)}$  randomly
4:  $\mathbf{x}^* \leftarrow \arg \max_{(\mathbf{x}, y) \in \mathcal{D}_0} y$ 
5: for  $t = 1$  to  $T_{\max}$  do
6:   // Phase 2: Adaptive  $\alpha$ -Scheduling
7:    $\alpha_t \leftarrow \alpha_0 \cdot \frac{\sqrt{t}}{\log(t+\epsilon)}$                                  $\triangleright$  Log-Sqrt Schedule (Eq. 15)
8:   // Phase 3: Inference (Warm Start)
9:   Run Collapsed Gibbs (Alg. 1) for  $S$  steps with  $\alpha_t$ , initialized from  $(\Theta^{(t-1)}, \mathbf{z}^{(t-1)})$ 
10:  Collect posterior samples  $\{\Theta^{(s)}, \mathbf{z}^{(s)}\}_{s=1}^S$ 
11:  Compute mixture moments  $\mu_{\text{mix}}(\mathbf{x})$ ,  $\sigma_{\text{mix}}(\mathbf{x})$  and weights  $w_k(\mathbf{x})$  (Thm. 8)
12:  // Phase 4: Acquisition Optimization
13:  Define  $\alpha_{\text{EI}}(\mathbf{x})$  per Eq. (11)
14:  Generate start points  $\mathcal{S}_{\text{init}} \leftarrow \{\text{UNIFORM}(\mathcal{X})\} \cup \{\text{CENTROIDS}(\mathbf{z})\} \cup \{\mathbf{x}^* + \boldsymbol{\delta}\}$ 
15:   $\mathbf{x}_{\text{new}} \leftarrow \arg \max_{\mathbf{x} \in \mathcal{S}_{\text{init}}} \text{L-BFGS-B}(\alpha_{\text{EI}}(\mathbf{x}))$ 
16:  // Phase 5: Evaluation & Update
17:   $y_{\text{new}} \leftarrow f(\mathbf{x}_{\text{new}}) + \varepsilon$ 
18:   $\mathcal{D}_t \leftarrow \mathcal{D}_{t-1} \cup \{(\mathbf{x}_{\text{new}}, y_{\text{new}})\}$ 
19:  if  $y_{\text{new}} > f(\mathbf{x}^*)$  then
20:     $\mathbf{x}^* \leftarrow \mathbf{x}_{\text{new}}$ 
21:  end if
22:  // Phase 6: Maintenance
23:  Update  $(\Theta^{(t)}, \mathbf{z}^{(t)})$  using the last MCMC sample
24:  Prune regimes where  $\sum_i \mathbb{I}(z_i = k) < 1$  or  $\pi_k < \epsilon$ 
25: end for

```

---

## Appendix C. Benchmarks

### C.1 Levy Function

The Levy function is characterized by a rugged surface with a high density of local minima, designed to challenge an optimizer's ability to resolve fine-grained structures. In the  $d$ -dimensional case, the function is defined as:

$$f(\mathbf{x}) = \sin^2(\pi w_1) + \sum_{i=1}^{d-1} (w_i - 1)^2 [1 + 10 \sin^2(\pi w_i + 1)] + (w_d - 1)^2 [1 + \sin^2(2\pi w_d)]$$

where  $w_i = 1 + \frac{x_i - 1}{4}$  for  $i = 1, \dots, d$ .

For our 2D visualization and validation, we consider  $x_i \in [-10, 10]$ . The landscape exhibits intense high-frequency oscillations (as shown in Figure 2), with the global minimum  $f(\mathbf{x}^*) = 0$  located at the interior point  $\mathbf{x}^* = (1, \dots, 1)$ .

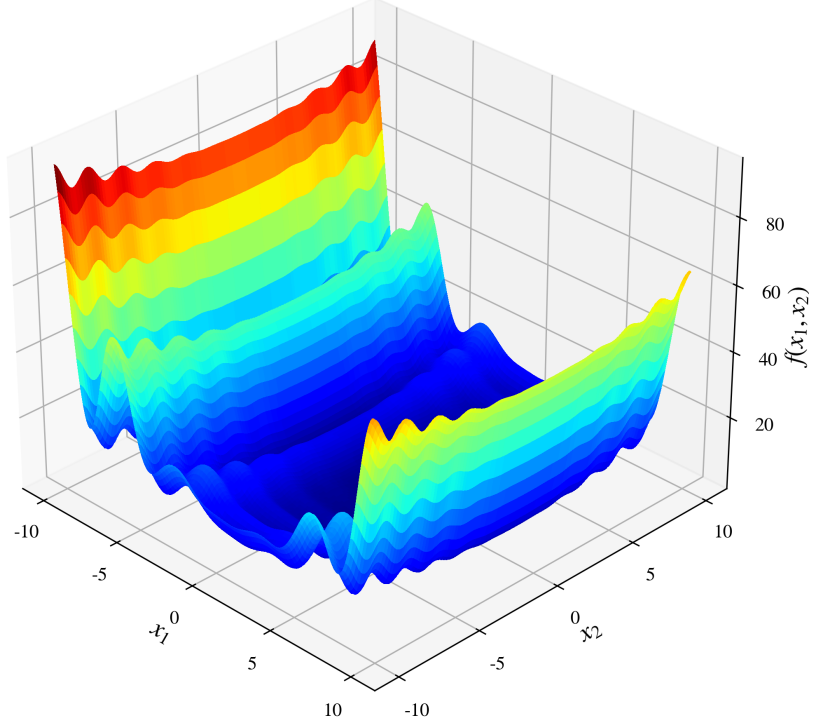


Figure 2: 3D landscape of the 2D Levy function, illustrating the dense clusters of local minima and rugged surface topology.

### C.2 Schwefel Function

The Schwefel function presents a deceptive landscape where the global optimum is geometrically isolated near the domain boundaries. This structure is particularly difficult for

stationary Gaussian Processes, as it penalizes methods that bias their search toward the central region of the domain. The mathematical representation is given by:

$$f(\mathbf{x}) = 418.9829d - \sum_{i=1}^d x_i \sin(\sqrt{|x_i|})$$

defined over the hypercube  $x_i \in [-500, 500]$ . As visualized in Figure 3, the function contains numerous sub-optimal peaks and basins.

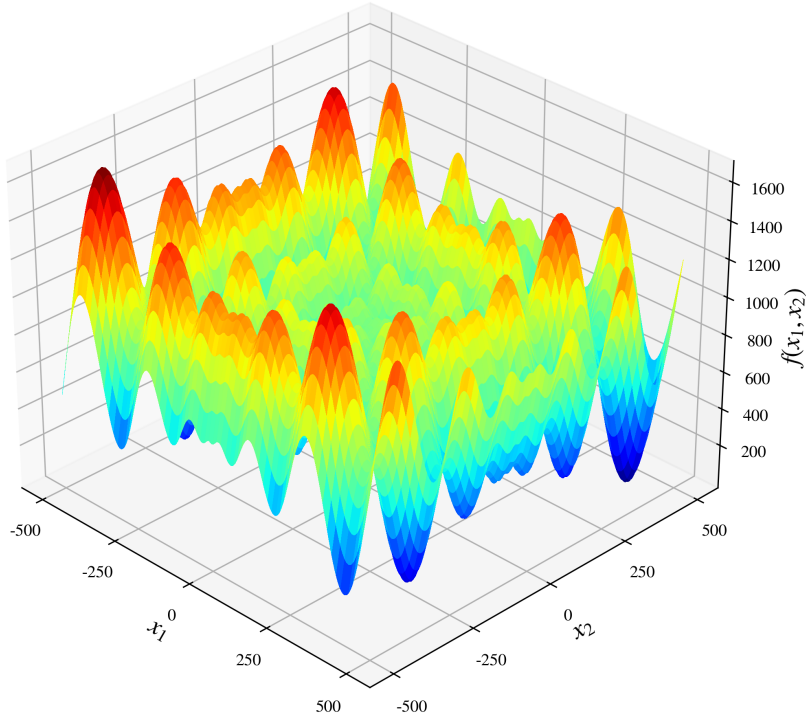


Figure 3: 3D landscape of the 2D Schwefel function, showcasing the deceptive local optima and the isolated nature of the global minimum.

### C.3 Molecular Conformer Optimization (12D)

The Molecular Conformer Optimization task serves as a high-dimensional, real-world benchmark to evaluate the scalability of RAMBO in pathological multi-modal landscapes. This problem involves finding the global minimum energy configuration of a pentadecane chain ( $C_{15}H_{32}$ ), where the state space is defined by  $d = 12$  internal dihedral (torsion) angles  $\boldsymbol{\theta} = (\theta_1, \dots, \theta_{12})$ .

**Mathematical Representation** The objective is to minimize the total potential energy  $E(\boldsymbol{\theta})$  of the conformer. We model this energy using the **MMFF94 force field** (Halgren,

1996), which can be decomposed into torsional contributions and non-bonded interactions:

$$E(\boldsymbol{\theta}) = \sum_{i=1}^{12} V_{tors}(\theta_i) + E_{non-bonded}(\mathbf{R}) \quad (38)$$

where  $V_{tors}(\theta_i)$  typically follows a periodic potential:

$$V_{tors}(\theta) = \sum_{n=1}^3 \frac{V_n}{2} [1 + \cos(n\theta - \gamma_n)] \quad (39)$$

The rotation around each  $C - C$  bond favors the  $180^\circ$  (anti) and  $\pm 60^\circ$  (gauche) orientations. This discrete preference induces a combinatorial explosion of  $3^{12} = 531,441$  potential conformational minima. These stable states are separated by high-energy steric barriers, creating a landscape characterized by sharp transitions and high-frequency oscillations.

**Implementation Details** To evaluate a configuration  $\boldsymbol{\theta}$ , we construct the molecular backbone using **RDKit** (Landrum et al., 2013). Crucially, to ensure a realistic energy landscape, we perform a **constrained geometry optimization**: the target dihedral angles  $\boldsymbol{\theta}$  are fixed using constraints, while all other degrees of freedom (bond lengths, angles, and Cartesian coordinates  $\mathbf{R}$ ) are relaxed to minimize the energy. This formulation prevents unrealistic steric clashes characteristic of rigid-body rotation and ensures the optimizer navigates a chemically valid potential energy surface.

**Problem Visualization** Figure 4 illustrates the geometric definition of a dihedral angle within the molecular chain, defined by a sequence of four consecutively bonded atoms (labeled Atoms 1–4). The rotation occurs around the central bond connecting Atom 2 and Atom 3, which serves as the rotation axis. This rotational motion determines the relative orientation of two intersecting planes: Plane 1, defined by Atoms 1, 2, and 3, and Plane 2, defined by Atoms 2, 3, and 4. The dihedral angle is the angle between these two planes.

#### C.4 Drug Discovery Screening (Cancer-6T2W, 50D)

We evaluate RAMBO on a drug discovery benchmark targeting the Colony-Stimulating Factor 1 Receptor (CSF1R) kinase domain (PDB ID: 6T2W) (Goldberg et al., 2020). CSF1R is a type III receptor tyrosine kinase that regulates tumor-associated macrophage differentiation and survival; its overexpression correlates with poor prognosis across multiple cancer types including breast, ovarian, and lung carcinomas (Wen et al., 2023). Pharmacological inhibition of CSF1R has emerged as a promising immunotherapeutic strategy, with pexidartinib (PLX3397) receiving FDA approval in 2019 for tenosynovial giant cell tumor (Tap et al., 2015).

The benchmark dataset, derived from the DrugImprover framework (Liu et al., 2023), comprises 1 million small molecules sampled from the ZINC15 database (Sterling and Irwin, 2015), each annotated with docking scores computed using the OpenEye FRED software (McGann, 2012). The BO objective is to *minimize* the docking score (more negative values indicate stronger predicted binding affinity). To enable continuous optimization, we represent molecules via 2048-bit Morgan fingerprints (Rogers and Hahn, 2010) compressed

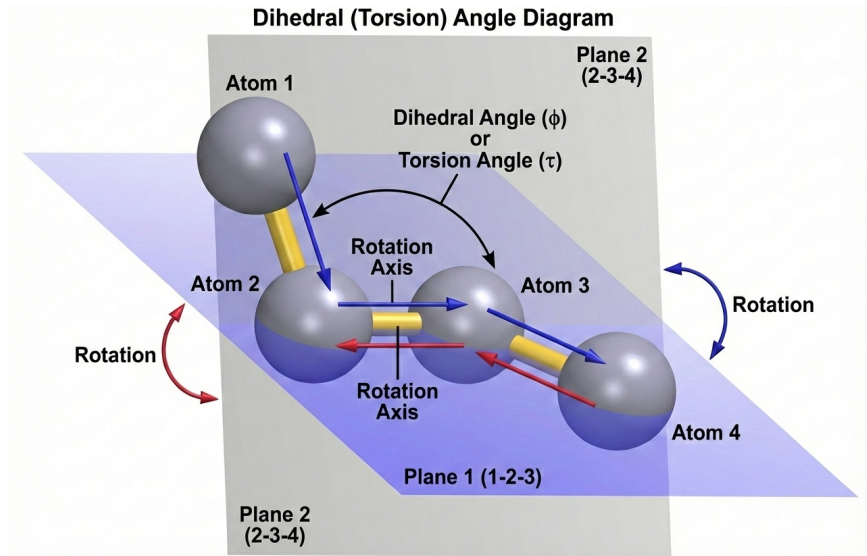


Figure 4: Dihedral (Torsion) Angle Diagram: The optimization space consists of 12 such rotational degrees of freedom, where steric hindrance between atoms 1 and 4 creates complex energy barriers.

to  $d = 50$  dimensions using Principal Component Analysis, following standard practice in latent-space molecular optimization (Gómez-Bombarelli et al., 2018).

This benchmark poses two challenges characteristic of real-world drug discovery: (1) **high dimensionality**—the 50D latent space necessitates efficient exploration strategies; and (2) **multi-regime structure**—distinct molecular scaffolds (e.g., different ring systems, functional groups, or pharmacophores) occupy disjoint regions of the latent space with fundamentally different structure-activity relationships (SAR). A single stationary GP cannot capture these scaffold-dependent landscapes, as binding affinity varies non-smoothly across chemical families. RAMBO’s regime-adaptive mechanism naturally partitions the chemical space into scaffold-specific clusters, enabling locally accurate surrogate modeling within each chemical series.

### C.5 Nuclear Fusion Reactor Design (ConStellaration, 81D)

We evaluate RAMBO on the ConStellaration benchmark (Cadena et al., 2025), a recently released dataset and optimization challenge for quasi-isodynamic (QI) stellarator design developed by Proxima Fusion in collaboration with Hugging Face. Stellarators are magnetic confinement devices that represent a promising path toward steady-state, disruption-free fusion energy (Gates et al., 2018; Helander, 2014). Unlike tokamaks, stellarators rely entirely on external electromagnetic coils to confine the plasma, avoiding current-driven instabilities but requiring complex three-dimensional magnetic field geometries that must be carefully optimized (Goodman et al., 2023).

**Dataset and Representation.** The ConStellaration dataset comprises approximately 158,000 QI-like stellarator plasma boundary configurations, each paired with ideal magneto-hydrodynamic (MHD) equilibria computed using VMEC++ (Hirshman and Whitson, 1983)

and associated performance metrics. The plasma boundary is parameterized by a truncated Fourier series in cylindrical coordinates  $(R, Z)$ :

$$R(\theta, \phi) = \sum_{m,n} R_{mn} \cos(m\theta - nN_{fp}\phi), \quad Z(\theta, \phi) = \sum_{m,n} Z_{mn} \sin(m\theta - nN_{fp}\phi),$$

where  $\theta$  and  $\phi$  are poloidal and toroidal angles, and  $N_{fp}$  is the number of field periods. Assuming stellarator symmetry (i.e.,  $R(\theta, \phi) = R(-\theta, -\phi)$  and  $Z(\theta, \phi) = -Z(-\theta, -\phi)$ ) and fixing the major radius  $R_{0,0} = 1$ , the optimization problem has  $d = 80$  degrees of freedom corresponding to the Fourier coefficients  $\{R_{mn}, Z_{mn}\}$ .

**Optimization Objective.** We adopt the “simple-to-build QI stellarator” benchmark, which seeks to maximize the quasi-isodynamic quality metric  $Q_{\text{QI}}$  while satisfying constraints on aspect ratio, rotational transform, and coil complexity. The QI property ensures that trapped particle orbits have vanishing average radial drift, which is critical for minimizing neoclassical transport and eliminating bootstrap currents that can destabilize the plasma (Helander and Nührenberg, 2009). Formally, the objective combines multiple physics targets including: (1) minimization of the effective ripple  $\epsilon_{\text{eff}}$  that governs neoclassical transport; (2) enforcement of poloidally closed  $|\mathbf{B}|$  contours characteristic of QI fields; and (3) penalization of high-curvature boundary shapes that would require complex coils to reproduce.

**Multi-Regime Structure.** Stellarator design exhibits highly nonlinear physics with abrupt transitions between qualitatively different magnetic field topologies. Small perturbations in boundary shape can trigger transitions between nested flux surfaces and magnetic islands, between regions of good and poor particle confinement, or between MHD-stable and unstable configurations. The optimization landscape is thus characterized by disconnected basins corresponding to fundamentally different plasma geometries—configurations with different numbers of field periods (1, 2, 3, 4, or 5 in the dataset), different magnetic well depths, and different elongation profiles occupy distinct regions of the Fourier coefficient space with incommensurable local curvature. This patchy landscape, where smooth regions of high confinement quality are interspersed with sharp transitions to unstable configurations, exemplifies the multi-regime structure that RAMBO is designed to capture. A single stationary GP with global hyperparameters cannot simultaneously model the smooth variation within each topology class and the abrupt transitions between them.

**Computational Cost.** Each function evaluation requires solving the 3D ideal-MHD equilibrium equations via VMEC++, which takes  $\mathcal{O}(\text{seconds to minutes})$  depending on resolution, making this a genuinely expensive black-box optimization problem well-suited for Bayesian optimization.

## Appendix D. Adaptive Concentration Parameter Scheduling

The concentration parameter  $\alpha$  governs regime creation in the Dirichlet Process: larger  $\alpha$  encourages more clusters, with  $\mathbb{E}[K_n | \alpha] \approx \alpha \log(n/\alpha + 1)$  (Antoniak, 1974). Prior work either fixes  $\alpha$  or learns it via MCMC (Rasmussen and Ghahramani, 2001), but for sequential optimization, the appropriate  $\alpha$  varies with data availability. With few observations, the data cannot reliably distinguish true regime structure from noise, and premature fragmentation leaves each GP expert with insufficient data for stable hyperparameter estimation. As observations accumulate, finer regime structure becomes statistically identifiable. This motivates a principled scheduling strategy: start conservative, then allow complexity to grow.

We formalize this intuition by matching the prior's expected complexity to a target regime discovery rate.

**Proposition 11** *Assume the number of discernible regimes  $K^*$  grows with sample size  $n$  at a polynomial rate  $\mathcal{O}(n^\beta)$  for  $\beta \in (0, 1)$ . To align the Dirichlet Process prior expectation  $\mathbb{E}[K_n | \alpha]$  with this target rate, the concentration parameter must scale as:*

$$\alpha^*(n) \propto \frac{n^\beta}{\log n}. \quad (40)$$

**Proof** Under the Chinese Restaurant Process representation, the expected number of clusters after  $n$  observations satisfies  $\mathbb{E}[K_n | \alpha] \approx \alpha \log(1 + n/\alpha)$  for  $n \gg 1$  (Antoniak, 1974). Suppose we seek a schedule  $\alpha_n$  such that  $\mathbb{E}[K_n | \alpha_n] \asymp n^\beta$ . Hypothesizing  $\alpha_n = c \cdot n^\beta / \log n$  for some constant  $c > 0$  and substituting:

$$\mathbb{E}[K_n | \alpha_n] = \frac{cn^\beta}{\log n} \log \left( 1 + \frac{n^{1-\beta} \log n}{c} \right). \quad (41)$$

As  $n \rightarrow \infty$ , the argument of the outer logarithm is dominated by  $n^{1-\beta}$ , yielding:

$$\mathbb{E}[K_n | \alpha_n] \approx \frac{cn^\beta}{\log n} \cdot (1 - \beta) \log n = c(1 - \beta)n^\beta. \quad (42)$$

Thus, the proposed scaling achieves the target growth rate  $\mathcal{O}(n^\beta)$ . ■

Guided by Proposition 11, we adopt a *square-root growth* assumption ( $\beta = 1/2$ ), motivated by the observation that distinct basins of attraction in multi-modal landscapes are discovered at a rate analogous to Heap's Law in information retrieval or the "square-root rule" in clustering heuristics (Heaps, 1978). This yields the **Log-Sqrt Schedule**:

$$\alpha_t = \alpha_0 \cdot \frac{\sqrt{t}}{\log(t + e)}, \quad (43)$$

where  $\alpha_0$  is a base concentration parameter (default  $\alpha_0 = 1.0$ ) and the offset  $e$  in the denominator ensures numerical stability at  $t = 1$ .

This schedule provides three desirable properties: (i) *early parsimony*—small  $\alpha_t$  initially prevents premature fragmentation when observations are sparse; (ii) *progressive refinement*—increasing  $\alpha_t$  enables fine-grained regime discovery as evidence accumulates; and (iii) *bias-variance balance*—the sub-linear growth rate avoids over-segmentation while permitting sufficient model flexibility. When  $\alpha_t$  changes between iterations, we warm-start Gibbs sampling from the previous assignments  $\mathbf{z}_{t-1}$  to preserve learned structure.